Pharmacological Research 182 (2022) 106322

Contents lists available at ScienceDirect

Pharmacological Research

journal homepage: www.elsevier.com/locate/yphrs

Preferential Gs protein coupling of the galanin Gal_1 receptor in the μ-opioid-Gal_1 receptor heterotetramer

Paulo A. De Oliveira [a,1], Estefanía Moreno [c,1], Nil Casajuana-Martin [d,1], Verònica Casadó-Anguera [c], Ning-Sheng Cai [a], Gisela Andrea Camacho-Hernandez [b], Hu Zhu [e], Alessandro Bonifazi [b], Matthew D. Hall [e], David Weinshenker [f], Amy Hauck Newman [b], Diomedes E. Logothetis [g], Vicent Casadó [c,*], Leigh D. Plant [g,*], Leonardo Pardo [d,*], Sergi Ferré [a,*]

[a] *Integrative Neurobiology Section, USA*
[b] *Medicinal Chemistry Section, National Institute on Drug Abuse, Intramural Research Program, National Institutes of Health, Baltimore, MD, USA*
[c] *Laboratory of Molecular Neuropharmacology, Department of Biochemistry and Molecular Biomedicine, Faculty of Biology and Institute of Biomedicine, University of Barcelona, Barcelona, Spain*
[d] *Laboratory of Computational Medicine, Biostatistics Unit, Faculty of Medicine, Autonomous University of Barcelona, Bellaterra, Spain*
[e] *Division of Preclinical Innovation, National Center for Advancing Translational Sciences, National Institutes of Health, Rockville, MD, USA*
[f] *Department of Human Genetics, Emory University School of Medicine, Atlanta, GA, USA*
[g] *Departments of Pharmaceutical Sciences, Chemistry and Chemical Biology and Center for Drug Discovery, School of Pharmacy at the Bouvé College of Health Sciences and College of Science, Northeastern University, Boston, MA, USA*

A R T I C L E I N F O

Keywords:
Opioid receptors
Galanin receptors
G protein coupled receptor oligomerization
Total internal reflection fluorescence microscopy

Chemical compounds studied in this article:
DAMGO (PubChem CID: 5462471)
Endomorphin-1 (PubChem CID: 5311080)
Galanin (PubChem CID: 16133823)
M40 (PubChem CID: 16133821)
M617 (PubChem CID: 16158157)
Naloxone (PubChem CID: 5284596)
Methadone (PubChem CID: 4095)
Fentanyl (PubChem CID: 3345)

A B S T R A C T

Recent studies have proposed that heteromers of μ-opioid receptors (MORs) and galanin Gal_1 receptors (Gal_1Rs) localized in the mesencephalon mediate the dopaminergic effects of opioids. The present study reports converging evidence, using a peptide-interfering approach combined with biophysical and biochemical techniques, including total internal reflection fluorescence microscopy, for a predominant homodimeric structure of MOR and Gal_1R when expressed individually, and for their preference to form functional heterotetramers when co-expressed. Results show that a heteromerization-dependent change in the Gal_1R homodimeric interface leads to a switch in G-protein coupling from inhibitory Gi to stimulatory Gs proteins. The MOR-Gal_1R heterotetramer, which is thus bound to Gs via the Gal_1R homodimer and Gi via the MOR homodimer, provides the framework for a canonical Gs-Gi antagonist interaction at the adenylyl cyclase level. These novel results shed light on the intense debate about the oligomeric quaternary structure of G protein-coupled receptors, their predilection for heteromer formation, and the resulting functional significance.

Abbreviations: A_{2A}R, adenosine A_2A receptor; AC, adenylyl cyclase; ANOVA, analysis of variance; BiFC, bimolecular fluorescence complementation; BRET, bioluminescence resonance energy transfer; cAMP, cyclic adenosine monophosphate; CODA-RET, complemented donor-acceptor resonance energy transfer; cryo-EM, cryo-electron microscopy; D_2R, dopamine D_2 receptor; DMEM, Dulbecco's modified Eagle's medium; EYFP, enhanced yellow variant of GFP; FBS, fetal bovine serum; Gal_1R, galanin Gal_1 receptor; FRET, fluorescence resonance energy transfer; GPCR, G protein-coupled receptor; HEK cells, human embryonic kidney cell line; mC, monomeric Cherry; mT, monomeric teal fluorescent protein 1; mVenus, monomeric Venus; MOR, μ-opioid receptors; MU cells, cell line expressing μ-opioid receptors; MU-GAL cells, cell line expressing μ-opioid receptors and galanin Gal_1 receptors; PEI, polyethylenimine; RLuc, *Renilla* Luciferase; TIRF, total internal reflection fluorescence; TM, transmembrane domain; VTA, ventral tegmental area; WT, wild-type; YFP, yellow fluorescence protein.

* Corresponding authors.
E-mail addresses: vcasado@ub.edu (V. Casadó), l.plant@northeastern.edu (L.D. Plant), Leonardo.Pardo@uab.cat (L. Pardo), sferre@intra.nida.nih.gov (S. Ferré).
[1] These authors contributed equally.

https://doi.org/10.1016/j.phrs.2022.106322
Received 7 April 2022; Received in revised form 18 June 2022; Accepted 19 June 2022
Available online 22 June 2022

1. Introduction

Although G protein-coupled receptor (GPCR) oligomerization represents an increasingly accepted concept [1–3], it is still under considerable debate [4–6], including concerns about the demonstration of GPCR homo and heteromers in artificial systems and their localization and functional significance in vivo [4,5]. Nevertheless, in some cases, the simultaneous use of different methodological approaches has provided significant convergent evidence for their functional presence in the experimental animal and for their putative role in pathological conditions and as targets for drug development [2].

Particularly valuable has been the use of disrupting synthetic peptides with the amino acid sequence of transmembrane domains (TMs) putatively involved in the intermolecular interactions between the GPCR units (protomers) of the oligomer. Using this strategy, several studies have provided decisive information about the quaternary structure of some GPCR heteromers and their functional and pharmacological properties, which could be ascertained with specific heteromer-disrupting peptides [7–10]. Three general conclusions could be drawn from those studies: that different TMs are involved in GPCR oligomerization; that GPCR heteromers provide the framework for emergent allosteric interactions; and that the same GPCR can display different oligomeric interfaces when forming heteromers with different GPCR, which determines different quaternary structures and therefore different properties [7–10].

It has been suggested that a common quaternary structure of a GPCR heteromer is a heterotetramer constituted by a homodimer coupled to a Gs/olf (Gs for short) protein and another homodimer coupled to a Gi/o (Gi for short) protein, which provides the framework for the canonical Gs-Gi antagonistic interaction at the adenylyl cyclase (AC) level, by which the activation of a Gi-coupled receptor inhibits the activation of AC by a Gs-coupled receptor [11]. AC is a plasma membrane protein with 12 TMs and 2 cytosolic catalytic domains that can separately interact with the α subunits of a Gs and a Gi protein [12]. It was shown that the canonical Gs-Gi antagonistic interaction at the AC level mediated by the Gs-coupled adenosine A_{2A} receptor ($A_{2A}R$) and the Gi-coupled dopamine D_2 receptor (D_2R) depends on the integrity of a macromolecular complex that includes the $A_{2A}R$-D_2R heterotetramer and AC (isoform AC5) [7].

The use of disrupting TM-peptides in native tissue preparations and in the experimental animal, including in vivo approaches, has also provided significant evidence for the localization and function of GPCR heteromers in the brain. One recent example is the localization of heteromers of μ-opioid receptors (MORs) and galanin Gal_1 receptors (Gal_1Rs) in the ventral tegmental area (VTA) [13,14], which represents a predominant population of MOR that mediates the dopaminergic effects of opioids [14]. Allosteric mechanisms in the MOR-Gal_1R heteromer determine the ability of Gal_1R ligands to decrease the affinity and efficacy of opioids and, importantly, a specific decrease in the potency of methadone [14]. This MOR-Gal_1R heteromer-dependent pharmacodynamic property of methadone provided a mechanistic explanation for its weaker dopaminergic effects, blunted euphoric properties, and lower abuse liability as compared with morphine and other opioids [14].

MOR is a Gi-coupled receptor and constitutes the main target for both the analgesic and unwanted side effects of opioids. Numerous studies have provided information about the structure and signaling properties of MOR, more often considered as a monomeric entity (for recent review, see ref. [15]). Initial studies supported a dimeric structure of the MOR [16–18], but this was challenged by more recent studies favoring its monomeric form [19–21]. Prior to the discovery of MOR--Gal_1R heteromers, other studies suggested the existence of heteromerization of MOR with different GPCRs, including the MOR-δ opioid receptor heteromer, claimed as a main target for the analgesic effects of opioids [2]. Gal_1R has also been described as preferentially coupled to Gi and potentially to Gq proteins [22]. Gal_1R localizes to several regions of the central nervous system and mediates many functions related to the neuromodulatory role of the neuropeptide galanin [22]. The cryo-electron microscopy (cryo-EM) structure of Gal_1R in its monomeric form bound to galanin and coupled to Gi has been recently resolved [23]. Similar to MOR, there is compelling evidence for the ability of Gal_1R to homomerize [24] and to form heteromers with several different GPCRs other than MOR [25].

The goal of the present study was to determine the quaternary structure of the MOR-Gal_1R heteromer using radioligand binding assays, bimolecular fluorescence complementation (BiFC), total internal reflection fluorescence (TIRF) microscopy, bioluminescence resonance energy transfer (BRET), complemented donor-acceptor resonance energy transfer (CODA-RET) and molecular modelling techniques. Based on the recent data indicating a predominant monomeric form of MOR and the common preferential Gi coupling of both MOR and Gal_1R, we initially favored the hypothesis of a heterodimeric structure. Unexpectedly, the results demonstrated a tetrameric quaternary structure of the MOR-Gal_1R heteromer constituted by a MOR homodimer coupled to Gi and a Gal_1R homodimer coupled to Gs. The MOR-Gal_1R heterotetramer provides the framework for the canonical Gs-Gi antagonist interaction at the AC level, and we found that the heteromerization-dependent switch of the coupling of Gal_1R from Gi to Gs involves a change in its homodimeric interface.

2. Materials and methods

2.1. Radioligand-binding experiments

2.1.1. Cell lines

Human embryonic kidney (HEK) cells stably expressing MORs (MU cells) or both MORs and Gal_1Rs (MU-GAL cells) were generated as described before [14]. Cells were maintained in culture with Dulbecco's modified Eagle's medium (DMEM) (Gibco, ThermoFisher Scientific, MA, USA) supplemented with 2 mM L-glutamine, 100 U/ml penicillin/streptomycin, MEM Non-Essential Amino Acid Solution (1/100), and 5% (v/v) heat-inactivated fetal bovine serum 5% fetal bovine serum (all supplements were from Gibco) and kept in an incubator at 37 °C and 5% CO_2 with selection antibiotics. MU cells were maintained with hygromycin B (50 μg/ml; Invitrogen, ThermoFisher Scientific) and MU-GAL cells with hygromycin B (50 μg/ml) and Geneticin (400 μg/ml; Gibco, ThermoFisher Scientific). Cells were kept below passage 20.

2.1.2. [^{3}H]Naloxone assays

MU and MU-GAL cell suspensions were disrupted with a Polytron homogenizer (PTA 7 rotor, setting 3; Kinematica, Basel, Switzerland) for two 5 s-periods in 10 volumes of 50 mM Tris-HCl buffer, pH 7.4, containing a protease inhibitor cocktail (Sigma-Aldrich, St. Louis, MO, USA). Membranes were obtained by centrifugation twice at 105.000 g for 45 min at 4 °C. The pellet was stored at − 80 °C, washed once more as described above and resuspended in 50 mM Tris-HCl buffer for immediate use. Membrane protein was quantified by the bicinchoninic acid method (Pierce Chemical Co., Rockford, IL, USA) using bovine serum albumin dilutions as standard. Binding experiments were performed with membrane suspensions (0.2 mg of protein/ml) at room temperature in 50 mM Tris-HCl buffer, pH 7.4, containing 5 mM $MgCl_2$. For MOR saturation-binding assays, membrane suspensions were incubated for 3 h with increasing concentrations of the MOR antagonist [^{3}H]naloxone (70 Ci/mmol, PerkinElmer, Boston, MA, USA). Non-specific binding was determined in the presence of 10 μM of the non-radiolabeled antagonist naloxone (Tocris, Bristol, United Kingdom). For competition-binding assays, membrane suspensions were incubated for 2 h with a constant free concentration of 2.4 nM of [^{3}H]naloxone and free increasing concentrations of the MOR agonists endomorphin-1 (Sigma-Aldrich) or DAMGO (Tocris). Free and membrane-bound ligands were separated by rapid filtration of 500 μl aliquots in a cell harvester (Brandel, Gaithersburg, MD, USA) through Whatman GF/C filters embedded in 0.3% polyethylenimine that were subsequently washed for 5 s with 5 ml of

ice-cold 50 mM Tris-HCl buffer. The filters were incubated with 10 ml of Ultima Gold MV scintillation cocktail (PerkinElmer, Waltham, Massachusetts, USA) overnight at room temperature and radioactivity counts were determined using a Tri-Carb 2800 scintillation counter (PerkinElmer).

2.1.3. [^{3}H]Galanin assays

Upon reaching 80–90% confluence, MU-GAL cells were harvested using pre-mixed Earle's Balanced Salt Solution (EBSS) with 5 mM EDTA (Life Technologies) and centrifuged at 3000 rpm for 10 min at 21 °C. The supernatant was removed, and the pellet was resuspended in 10 ml hypotonic lysis buffer (5 mM $MgCl_2$, 5 mM Tris, pH 7.4 at 4 °C) and centrifuged at 14,500 rpm for 30 min at 4 °C. The pellet was then resuspended in fresh binding buffer. A Bradford protein assay (Bio-Rad) was used to determine the protein concentration, and membrane aliquots were frozen in fresh binding buffer at − 80 °C for future use. The binding buffer was made of 50 mM Tris and 5 mM $MgCl_2$ at pH 7.4. On test day, the radioligand [^{3}H]-galanin (NOVANDI Chemistry AB, 98 Ci/mmol SA) was diluted into half-log serial dilutions using fresh binding buffer. Membranes were diluted in fresh binding buffer at a stock concentration of 0.3 mg/ml. Radioligand hot saturation experiments were conducted in 96-well plates containing 300 µl fresh binding buffer, 50 µl of diluted radioligand concentrations, 100 µl of membranes (final amount of 30 µg/well for MU-GAL cells), and 50 µl of either 30% DMSO vehicle (total binding) or 100 µM of the galanin receptor ligand M40 (10 µM final concentration, non-specific binding). All dilutions were tested in triplicate and the reactions incubated for 2 h at room temperature. The reaction was terminated by filtration through a Perkin Elmer Uni-Filter-96 GF/B or GF/C, presoaked for 2 h in 0.5% polyethylenimine, using a Brandel 96-Well Plates Harvester Manifold (Brandel Instruments). The filters were washed 3 times with 3 ml (3 ×1 ml/well) of ice-cold binding buffer. 65 µl Perkin Elmer MicroScint20 Scintillation Cocktail was added to each well and filters were counted using a Perkin Elmer MicroBeta Microplate Counter.

2.1.4. Data analysis

Data were analyzed according to the 'dimer receptor model' (see text and refs. [26,27]). In competition experiments, the model analyzes the interactions of the radioligand with a competing ligand and it provides the affinity of the competing ligand for the first protomer in the unoccupied dimer (K_{DB1}), the affinity of the competing ligand for the second protomer when the first protomer is already occupied by the competing ligand (K_{DB2}) or the radioligand (K_{DAB}), and an index of cooperativity of the competing ligand (D_{CB}). A positive or negative value of D_{CB} implies either an increase or a decrease in affinity of K_{DB2} versus K_{DB1} and its absolute value provides a measure of the degree of increase or decrease in affinity. Radioligand binding curves were analyzed by nonlinear regression using the commercial Grafit curve-fitting software (Erithacus Software, Surrey, UK), by fitting the binding data to the mechanistic dimer receptor model, as described in detail elsewhere [27].

Saturation assays data must be fitted to Eq. (1).

$$A_{bound} = \frac{\left(K_{DA2}\,A + 2\,A^2\right)\,R_T}{\left(K_{DA1}K_{DA2} + K_{DA2}A + A^2\right)} \quad (1)$$

where A represents the free radioligand concentration, R_T is the total amount of receptor dimers, and K_{DA1} and K_{DA2} are the macroscopic equilibrium dissociation constants describing the binding of the first and the second radioligand molecule to the receptor homodimer. Nevertheless, in non-cooperative conditions, $K_{DA2}/K_{DA1} = 4$. Then, K_{DA1} is enough to characterize the binding. Therefore, Eq. (1) can be reduced to Eq. (2):

$$A_{bound} = \frac{2AR_T}{2K_{DA1} + A} \quad (2)$$

To calculate the macroscopic equilibrium dissociation constants from competition experiments, the following general equation (Eq. (3)) must be applied:

$$A_{bound} = \frac{\left(K_{DA2}A + 2A^2 + \frac{K_{DA2}AB}{K_{DAB}}\right)R_T}{K_{DA1}K_{DA2} + K_{DA2}A + A^2 + \frac{K_{DA2}AB}{K_{DAB}} + \frac{K_{DA1}K_{DA2}B}{K_{DB1}} + \frac{K_{DA1}K_{DA2}B^2}{K_{DB1}K_{DB2}}} \quad (3)$$

where B represents the assayed competing compound concentration. However, in absence of cooperativity of the radioligand, Eq. (3) can be simplified, since: $K_{DA2} = 4\,K_{DA1}$ (Eq. (4)):

$$A_{bound} = \frac{\left(4K_{DA1}A + 2A^2 + \frac{4K_{DA1}AB}{K_{DAB}}\right)R_T}{4{K_{DA1}}^2 + 4K_{DA1}A + A^2 + \frac{4K_{DA1}AB}{K_{DAB}} + \frac{4{K_{DA1}}^2B}{K_{DB1}} + \frac{4{K_{DA1}}^2B^2}{K_{DB1}K_{DB2}}} \quad (4)$$

2.2. Expression vectors and fusion proteins

Sequences encoding amino acids residues 1–229 and 230–311 of *Renilla* Luciferase (RLuc8 variant) and amino acid residues 1–155 and 156–238 of the monomeric Venus variant (mVenus) of the yellow fluorescence protein (YFP) were subcloned in pcDNA3.1 vector to obtain complementary RLuc and YFP hemi-truncated proteins (nRLuc, cRLuc, nYFP, and cYFP). To obtain receptors fused to the full RLuc or to the different hemi-truncated proteins, human cDNAs for MOR and Gal_1R cloned into pcDNA3.1 were amplified without their stop codons using sense and antisense primers harboring *Eco*RV and *Kpn*I to clone MOR and *Eco*RI and *Kpn*I to clone Gal_1R. The amplified fragments were subcloned to be in-frame with restriction sites of pcRLuc-N1 vector (pRLuc-N1 PerkinElmer, Wellesley, MA, USA), pEYFP-N1 vector (enhanced yellow variant of GFP; Clontech, Heidelberg, Germany), pcDNA3.1-nRLuc, pcDNA3.1-cRLuc pcDNA3.1-nYFP or pcDNA3.1-cYFP, to provide plasmids that express the receptor fused to RLuc, YFP, nRLuc, cRLuc, nYFP or cYFP on the C-terminal end of the receptor. The following human G protein constructs were used: Gαi1-YFP (with YFP, mVenus variant, inserted at position 91), Gαs-YFP (with YFP, mVenus variant, inserted at position 154 of Gαs, short isoform), and Gαq-YFP (with YFP, mVenus variant, inserted at position 97 of Gαs), untagged Gβ1, and untagged Gγ2. Mutagenesis of Gαs-YFP and Gαi1-YFP was performed using QuikChange Lightning single site-directed mutagenesis kits (Agilent, Santa Clara, CA, USA). Mutant Gαs-YFP, with a deletion of the thirteen-amino acid sequence TTPEDATPEPGED was generated by using the primer gaatttgctcgctacccacgcgtgacccgg. Mutant Gαi1-YFP, with the insertion of the same thirteen-amino acid sequence in the homologous site was generated by using the primer atccagaatatgcaggatcaactactcctgaggatgctactcccgagcccggagaggacaacacatatgaagaggcagc. Primers were synthesized by Integrated DNA Technologies, Inc. (IDT, San Diego, CA, USA). All the constructs were confirmed by sequencing analysis. Several constructs were shared by.

C. Gales at INSERM (Toulouse, France; Gαi1 construct) and N. Lambert (Georgia Regents University, Augusta, GA; Gαs). The expression of constructs was tested by confocal microscopy and the receptor-fusion protein functionality by ERK1/2 phosphorylation.

2.3. Cell cultures and transient transfection

HEK 293 T cells obtained from ATCC were grown in Dulbecco's modified Eagle's medium (DMEM) (Gibco) supplemented with 2 mM L-glutamine, 100 µg/ml sodium pyruvate, 100 U/ml penicillin/streptomycin, MEM non-essential amino acid solution (1/100), and 5% (v/v) heat inactivated fetal bovine serum (FBS) (all supplements were from Invitrogen, Paisley, Scotland, UK). Cells were maintained at 37 °C in an atmosphere of 5% CO2 and were routinely tested for mycoplasma. For transient transfection, HEK-293 T cells growing in 10-cm or 6-well dishes were transfected with the corresponding cDNAs by the polyethylenimine (PEI, Sigma) method. All constructs were confirmed by sequencing analysis. Cells were incubated (4 h) with the corresponding

cDNA together with PEI (5.47 mM in nitrogen residues) and 150 mM NaCl in a serum-starved medium. After 4 h, the medium was changed to a fresh complete culture medium. Forty-eight hours after transfection, cells were washed twice in quick succession in Hank's balanced salts solution [containing the following (in mM): 137 NaCl, 5 KCl, 0.34 Na_2HPO_4 x12H_2O, 0.44 KH_2PO_4, 1.26 $CaCl_2$ x2H_2O, 0.4 $MgSO_4$ x7H_2O, 0.5 $MgCl_2$, 10 HEPES, pH 7.4], supplemented with 0.1% glucose (w/v), detached and resuspended in the same buffer. Cell number was controlled by determining sample protein concentration using a Bradford assay kit (Bio-Rad, Munich, Germany) with bovine serum albumin (BSA) dilutions as standards.

2.4. HIV TAT-fused TM peptides

Peptides with the amino acid sequence of TMs of the human MOR and human Gal_1R were used as oligomer destabilizing agents, as previously demonstrated [7–10,13,14]. To facilitate the insertion into the plasma membrane, the TM peptides were fused to the cell-penetrating HIV transactivator of transcription (TAT) peptide (YGRKKRRQRRR) [28]. A TAT-TM peptide can be inserted effectively into the plasma membrane because of the penetration capacity of the TAT peptide and the hydrophobic property of the TM peptide [29]. To obtain the right orientation of the membrane-inserted peptide, the TAT peptide was fused to the C-terminus of peptides with the amino acid sequence of TM 1, TM 3, TM 5, and TM 7 of MOR or the Gal_1R (TM1, TM3, TM5, and TM7 peptides, respectively) or to the N terminus of TM 2, TM 4, and TM 6 of MOR or the Gal_1R (TM2, TM4, and TM6 peptides, respectively). All peptides were synthesized by Genemed Synthesis, Inc. Their sequences were as follows:TAITIMALYSIVCVVGLFGNFLVMYYGRKKRRQRRR for TM1 of MOR,YGRKKRRQRRRIYIFNLALADALATSTLPFQSVNYL for TM2 of MOR,KIVISIDYYNMFTSIFTLCTMSVYGRKKRRQRRR for TM3 of MOR,YGRKKRRQRRRAKIINVCNWILSSAIGLPVMFM for TM4 of MOR, ENLLKICVFIFAFIMPVLIITVCYGYGRKKRRQRRR for TM5 of MOR, YGRKKRRQRRRITRMVLVVVAVFIVCWTPIHIYVIIKA for TM6 of MOR, FQTVSWHFCIALGYTNSCLNPVLYYGRKKRRQRRR for TM7 of MOR, LVVFGLIFALGVLGNSLVITVYGRKKRRQRRR for TM1 of Gal_1R, YGRKKRRQRRRNLFILNLSIADLAYLLFCIPF for TM2 of Gal_1R, FIHYFFTVSMLVSIFTLAAMSVYGRKKRRQRRR for TM3 of Gal_1R, YGRKKRRQRRRALLGVGCIWALSIAMASPVAY for TM4 of Gal_1R, VVCTFVFGYLLPLLLICFCYAYGRKKRRQRRR for TM5 of Gal_1R, YGRKKRRQRRRVLVVVVVFGISWLPHHIIHLW for TM6 of Gal_1R, FGVFPLTPASFLFRITAHCLAYGRKKRRQRRR for TM7 of Gal_1R.

2.5. Bimolecular fluorescence complementation (BiFC)

HEK-293 T cells were transiently co-transfected with the cDNA encoding the corresponding receptor fused to n-YFP and the receptor fused to c-YFP. The amount of transfected cDNA was 4 μg for each construct, except in the experiments where non-fused receptors were additionally transfected: 4 μM, 4 μM and 16 μM in the experiments with MOR-cYFP, MOR-nYFP and Gal_1R, respectively; and 4 μM, 4 μM and 1 μM in the experiments with Gal_1R-cYFP, Gal_1R-nYFP and MOR, respectively. After transfection (48 h) cells were treated or not with the indicated TM peptides (4 μM) for 4 h at 37 °C. Reconstituted YFP expression was quantified by distributing the cells (20 μg protein) in 96-well microplates (black plates with a transparent bottom, Porvair, King's Lynn), and emission fluorescence at 530 nm was read in a Fluo Star Optima Fluorimeter (BMG Labtechnologies) equipped with a high-energy xenon flash lamp, using a 10 nm bandwidth excitation filter at 400 nm reading. Protein fluorescence expression was determined as fluorescence of the sample minus the fluorescence of cells not expressing the fusion proteins (basal). Cells expressing Gal_1R-cYFP and nYFP or MOR-nYFP and cYFP showed similar fluorescence levels to non-transfected cells.

2.6. cAMP formation

HEK-293 T cells were transiently co-transfected with the cDNA encoding MOR-RLuc (1.2 μg) and/or Gal_1R-YFP (4.8 μg) and 48 h after they were analyzed for cyclic adenosine monophosphate (cAMP) formation experiments. Homogeneous time-resolved fluorescence energy transfer (HTRF) assays were performed using the Lance Ultra cAMP kit (PerkinElmer, Waltham, MA), based on competitive displacement of a europium chelate-labelled cAMP tracer bound to a specific antibody conjugated to acceptor beads. The optimal cell density for an appropriate fluorescent signal was first established by measuring the time-resolved fluorescence resonance energy transfer (FRET) signal determined as a function of forskolin concentration using different cell densities. Forskolin dose-response curves were related to the cAMP standard curve, to establish a cell density with a response covering most of the dynamic range of the cAMP standard curve. Cells were not treated or treated with vehicle or 4 μM of the indicated TM peptides for 4 h at 37°C in an atmosphere of 5% CO_2. Cells were then grown (1000 cells/well) in white ProxiPlate 384-well microplates (PerkinElmer, Waltham, MA) in medium containing 50 μM zardaverine, stimulated with agonists (all at 0.5 μM) for 10 min before adding 0.5 μM forskolin or vehicle and incubated for an additional 15-min period. Fluorescence at 665 nm was analyzed on a PHERAstar Flagship microplate reader equipped with an HTRF optical module (BMG Lab technologies, Offenburg, Germany).

2.7. β-arrestin recruitment assay

A PathHunter® CHO-K1 Gal_1R β-arrestin cell line (Eurofins DiscoverX, Fremont, CA) was used to determine agonist-induced β-arrestin recruitment. PathHunter® β-arrestin GPCR cell lines co-express a ProLink™ (PK) tagged GPCR (here, human Gal_1R) and an Enzyme Acceptor (EA) tagged β-arrestin. Activation of the GPCR-PK induces β-arrestin-EA recruitment, forcing complementation of the two β-galactosidase enzyme fragments (EA and PK). The resulting functional enzyme hydrolyzes substrate to generate a chemiluminescent signal. Cells were maintained in Ham's F-12 medium (ThermoFisher Scientific) supplemented with 2 mM L-glutamine, 100 U/ml penicillin/streptomycin, geneticin (800 μg/ml), hygromycin B (300 μg/ml) and 10% FBS (all supplements were from ThermoFisher Scientific). The PathHunter® Detection Kit (Eurofins DiscoverX) was used for the β-arrestin recruitment assay. Cells were harvested with StemPro Accutase Cell Dissociation Reagent (ThermoFisher Scientific) and seeded in 1536-well white flat bottom plates (Greiner, Monroe, NC) at a density of 1000 cells/3 μl/well in AssayComplete Cell Plating Reagent 2 (Eurofin DiscoverX). After incubating at 37 °C, 5% CO_2 overnight, 20 nl/well of galanin or M40 were transferred to the wells by Echo 555 Acoustic Liquid Handler (Labcyte, San Jose, CA). Ninety minutes after, 1.5 μl/well of PathHunter detection reagent (Eurofin DiscoverX) was added to the microplates with the BioRAPTR FRD dispenser (Beckman Coulter, Brea, CA). The detection reagent was prepared by mixing Galacton Star Substrate, Emerald II solution and PathHunter buffer (supplied by the assay kit; at 1:5:19), added to the microplates and, after incubation at room temperature for 1 h, the luminescent signal was detected on a ViewLux plate reader (PerkinElmer, Waltham, MA).

2.8. Calcium mobilization assay

A CHO-K1-Gαqi5 Gal_1R stable cell line (Multispan Inc., Hayward, CA) was used to determine agonist-induced calcium mobilization. The cell line stably expresses human Gal_1R and the mutant Gαqi5, where the five Gαq C-terminal amino acids have been replaced with those from the Gαi protein, allowing Gαi-coupled receptors to respond to an agonist via elevation of intracellular calcium. Cells were maintained in DMEM-F12 medium (ThermoFisher Scientific) supplemented with 2 mM L-glutamine, 100 U/ml penicillin/streptomycin, puromycin (800 μg/ml), hygromycin B (150 μg/ml) and 10% FBS (all supplements were from

ThermoFisher Scientific). Cells were harvested with StemPro Accutase Cell Dissociation Reagent (ThermoFisher Scientific) and seeded in 1536-well μClear® black microplates (Greiner, Monroe, NC) at a density of 1000 cells/3 μl/well in DMEM-F12 medium. After incubating at 37 °C, 5% CO_2 overnight, 3 μl Calbryte™ 520NW dye-loading solution (AAT Bioquest, Sunnyvale, CA) was added into each well. The dye-loading solution was prepared by mixing 1xHHBS buffer, 10xPluronic® F127 Plus and Calbryte™ 520NW stock solution (supplied by the assay kit). The dye-loading plates were incubated at 37 °C, 5% CO_2 for 30 min, and then incubated at room temperature for another 15–30 min. The microplates were loaded on the FLIPR Tetra High-Throughput Cellular Screening System (Molecular Devices, San Jose, CA). The baseline fluorescence signal was measured for 10 s, 10 nl of either galanin or M40 were transferred into each well and the fluorescence signals were measured for 3 min at 1-second interval. The relative fluorescence unit (RFU) was calculated by maximum signal – minimum signal.

2.9. Bioluminescence resonance energy transfer (BRET)

HEK-293 T cells were co-transfected with MOR-RLuc (0.25 μg) or Gal_1R-RLuc (0.25 μg), as well as with Gαi1-YFP, Gαq-YFP or Gαs-YFP (5 μg) and untagged Gβ1 (4.5 μg) and Gγ2 (5 μg). Experiments were performed approximately 48 h after transfection. The transient transfected cells were collected, washed, and resuspended in Dulbecco's PBS (DPBS) with 0.1% glucose and 200 μM sodium bisulfite. Approximately 200,000 cells/well were distributed in 96-well plates, and 5 μM coelenterazine H (NanoLight Technology) was added. Fluorescence of the acceptor was quantified (excitation at 500 nm and emission at 540 nm for 1-s recording) to confirm the constant expression level across experiments. Two minutes after the addition of coelenterazine, increasing concentrations of different MOR or Gal_1R agonists were added to different wells. The plate was read after agonist addition using a Mithras LB940 microplate reader (Berthold Technologies). BRET signal from cells was calculated as the ratio of the light emitted by Rluc8 at 485 nm to that emitted by YFP (mVenus variant) at 530 nm. A BRET change was defined as the BRET ratio for the corresponding drug minus the BRET ratio in the absence of the drug. E_{max} and EC_{50} values are expressed as the basal subtracted BRET change in the concentration-response graphs.

2.10. Complemented donor-acceptor resonance energy transfer (CODA-RET)

HEK-293 T cells co-transfected with MOR-cRLuc (3.3 μg) and Gal_1R-nRluc (1.6 μg), and co-transfected with either Gαi1-YFP, Gαq-YFP or Gαs-YFP (5 μg) subunit and untagged Gβ1 (4.5 μg) and Gγ2 (5 μg). 48 h after transfection the cells were harvested, washed, and resuspended in phosphate-buffered saline (PBS). About 200,000 cells/well were distributed in 96-well plates, and 5 μM coelenterazine H was added to each well. Two minutes after the addition of coelenterazine, increasing concentrations of different MOR or GA1R agonists were added to each well. Fluorescence of the acceptor was quantified (excitation at 500 nm and emission at 540 nm for 1-s recording) in the Mithras LB940 reader to confirm the constant expression level across experiments. In parallel, BRET signal from the same batch of cells was determined as the ratio of the light emitted by YFP (mVenus variant; 530 nm) over RLuc (485 nm). Results were calculated for the BRET change (BRET ratio for the corresponding drug minus BRET ratio in the absence of the drug) 5 min after addition of the agonists. Nonlinear fitting to obtain E_{max} and EC_{50} values for all CODA-RET, BRET and statistical analysis were performed with GraphPad Prism 7 software (La Jolla, CA).

2.11. Total internal reflection fluorescence (TIRF) microscopy

Gal_1R and MOR receptors were tagged at the C-terminus with mTFP1 and mCherry, respectively, and imaged at the surface of live HEK-293 T cells by TIRF microscopy. Cells were seeded to #1.5 glass coverslips, transfected as described above, and studied after 24–32 h in a bath solution comprising (in mM): 140 NaCl, 4 KCl, 1.8 $CaCl_2$, 1 $MgCl_2$, 8 glucose, 5 HEPES, with the pH set to 7.4 with NaOH. Fluorophore monomeric teal FP1 (mTFP1) was excited by a 445-nm laser and mCherry by a 561-nm laser (Coherent, Santa Clara, CA). The beams were conditioned for coherence with custom built Keplerian beam expanders upstream of laser cleanup filters (445/10 nm and 561/10x). Laser lines were tuned to provide 10 mW of incident light on a micro mirror positioned below a high numerical-aperture apochromat objective (60x, 1.5 NA; Olympus, Waltham, MA) mounted on an RM21 microscope frame equipped with a piezo-driven nanopositioning stage (MadCity Labs., Madison, WI). The emission of mTFP1 and mCherry were isolated from the excitation beam by an exit micro mirror and a ring-diagram positioned below the micro mirror assembly. When mTFP1 and mCherry were imaged simultaneously, the emission was split by 510-nm dichroic mirrors placed downstream of parallel 480/40 nm and 620/60 nm bandpass filters. The fluorophores were imaged using a back illuminated sCMOS camera (Teledyne Photometrics, Tucson, AZ) controlled by Micro-Manager freeware (UCSF). All filters and mirrors were from Chroma (Bellow Falls, VT). Lenses, pinholes and diaphragms were from ThorLabs (Newton, NJ). Tetrapsec beads (Thermo, Waltham, MA) were routinely imaged to map the sCMOS chip and to calibrate the evanescent field depth to 100 nm. To assess stoichiometry, fluorophores were photobleached by continual excitation. Data were captured as 16-bit movies of up to 600 frames acquired at 1 Hz. When mT-Gal1R and mC-MOR were studied in the same cell, the data for each fluorophore were captured simultaneously to a mapped sCMOS chip, saved as separate image stacks and processed in an identical manner. Images were background corrected by subtracting the mean of 5 fully bleached frames from the end of each stack analyzed [30]. Fluorescent particles were defined as a discrete 3 × 3-pixel region around a pixel of maximum intensity, as before and misalignment was corrected in ImageJ using StackReg. Co-localization of partner pixels from the two stacks of images was defined as the presence of both fluorophores with at least 30% of maximum fluorescence levels recorded in that region of interest, as before [31].

2.12. Computational methods

Computational models of MOR-MOR and Gal_1R-Gal_1R homodimers were built via the TM 4/5 dimeric interface of the β_1-adrenergic receptor (PDB code 4GPO) [32] or via the TM 5/6 interface of the MOR structure (4DKL) [18], using the crystal structure of MOR (4DKL), a MOR-based homology model of Gal_1R in an inactive state, and the recent cryo-EM structure of Gal_1R in an active state (7WQ3) [23]. The MOR-Gal_1R heterodimer was constructed via the TM 5/6 interface of the MOR structure. The complex of MOR with Gi was modeled using the corresponding cryo-EM structure (6DDF) [33]. The complexes of Gal_1R with G proteins were modeled using the structure 7WQ3 (Gal_1R in complex with Gi) [23], or cholecystokinin A receptor in complex with Gs (7MBX) or Gq (7EZM) [34] as templates. Modeling was performed using Modeller 10.1 [35] and AmberTools19.

2.13. Statistical analysis

In binding assays, goodness of fit was tested according to a reduced chi-squared value given by the regression program. The test of significance for two different model population variances was based upon the F-distribution using built-in functions in GraFit software. A probability greater than 95% ($p < 0.05$) was considered the criterion to select a more complex model (cooperativity) over the simplest one (non-cooperativity). Other statistical analyses were performed using GraphPad Prism 6 software. Differences between experimental group pairs were analyzed with two-tailed paired Student's *t*-test. Differences among more than two groups of results were performed by one-way analysis of variance (ANOVA) followed by Dunnett's or Tukey's multiple

comparisons tests. Sample size estimation was based on our previous studies with radioligand binding experiments, biophysical techniques and signaling in mammalian transfected cells, which favored an n between 5 and 7 to demonstrate statistical differences between different experimental groups [7–9,13,14]. In addition, sample replicates (the average of triplicates as n = 1) were used in most experiments to moderate the experimental variability. Data were presented as means ± standard error of the means (S.E.M.) or ± standard deviations (S.D.), as indicated in the respective figure legend. A level of $p < 0.05$ was considered as critical for assigning statistical significance.

3. Results

3.1. Negative cooperativity of agonist binding indicates homodimerization of MOR in the presence or absence of Gal_1R

Radioligand binding experiments have classically shown the existence of two apparent populations of GPCRs, with high and low affinities for the agonist. This has commonly been observed with a shallow or even biphasic curve in radiolabeled antagonist versus agonist competition experiments. Although it has been generally assumed that these results indicate the existence of G protein-coupled and uncoupled states of the GPCR, seminal studies by Redka et al. [36,37] demonstrated that, within the physiological range of an excess of G proteins versus GPCRs, these apparently different populations of GPCRs correspond to negative binding cooperativity of the agonist binding to the different protomers of GPCR oligomers. Application of mathematical models that consider GPCRs as homodimers to the analysis of radioligand binding data, such as the 'dimer receptor model' [26], provides values of the two agonist binding affinities (K_{DB1} and K_{DB2}) that are significantly more robust (less dependent on the experimental conditions) than those of monomer-G protein models (K_H and K_L) [1,6,27,38]. The 'dimer receptor model' also introduces a dimer cooperativity index (D_{CB}). $D_{CB} = 0$ implies no agonist cooperativity, whereas positive and negative values imply positive and negative cooperativity, respectively [1,6,27,38].

Analysis of radioligand binding data with the 'dimer receptor model' can therefore be used to interrogate the predominant monomeric or dimeric structure of GPCRs, which we applied to the question of a monomeric versus dimeric structure of MOR. Competitive inhibition experiments of the radiolabeled MOR antagonist [^{3}H]naloxone (2.4 nM) versus increasing concentrations of the endogenous MOR agonist endomorphin-1 (Figs. 1a and 1b) or [^{3}H]naloxone (1.1 nM) versus increasing concentrations of the exogenous MOR agonist DAMGO (Suppl. Fig. 1) were performed in membrane preparations from two previously described and characterized HEK-293 T cell lines stably expressing either MOR alone (MU cells) or co-expressing Gal_1R (MU-GAL cells) [14]. For both cell lines and for both MOR agonists, a significantly better fit was obtained for biphasic versus monophasic curves ($p < 0.05$ in all cases). Endomorphin-1 bound to the MOR with two affinities and negative cooperativity, both in MU cells (Fig. 1a, in means±S.E.M.; K_{DB1}=4.1 ± 0.6 nM; K_{DB2}=130 ± 20 nM; D_{CB}=−0.9; n = 9) and MU-GAL cells (Fig. 1b, K_{DB1}=1.0 ± 0.2 nM; K_{DB2}=40 ± 10 nM; D_{CB}=−1; n = 7). Very similar qualitative results were obtained with DAMGO (Suppl. Fig. 1). Saturation experiments with [^{3}H]naloxone were performed to analyze possible differences in affinity of [^{3}H]naloxone in MU cells and MU-GAL cells, which showed K_{DA1} values (in means±S.E.M) of 1.4 ± 0.2 and 1.6 ± 0.3 nM, respectively (n = 3). MU-GAL cells were additionally characterized for the affinity of [^{3}H]galanin binding sites in saturation experiments, which showed K_{DA1} values (in means±S.E.M) of 1.2 ± 0.1 nM (n = 3; Suppl. Fig. 1). Altogether, radioligand binding experiments are indicative of a preferential oligomeric structure of MOR with the same radioligand binding characteristics, whether or not it forms or not heteromers with Gal_1R.

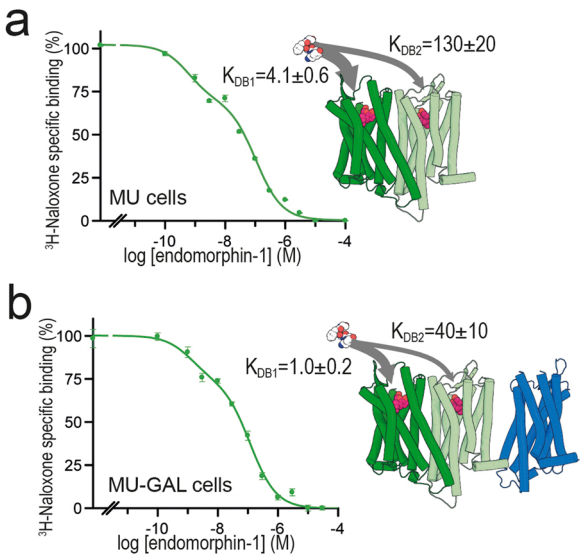

Fig. 1. Negative cooperativity of endomorphin-1 in radioligand binding experiments. Representative competitive inhibition curves of [^{3}H]naloxone/endomorphin-1 in HEK-293 T cell lines stably expressing either MOR alone (MU cells; **a**) or with Gal_1R (MU-GAL cells; **b**); data was adjusted with the 'dimer-receptor model', which provided a significantly better biphasic versus monophasic fit for both cell lines ($p < 0.05$ in all cases; see Materials and Methods), with two affinities (K_{DB1} and K_{DB2}; n = 7–9, with triplicates) and negative cooperativity ($D_{CB} \approx -1$), indicative of a predominant population of MOR homodimers.

3.2. Homomeric and heteromeric TM interfaces in the MOR-Gal_1R heteromer

The putative heterotetrameric structure of the MOR-Gal_1R heteromer was evaluated by BiFC experiments in combination with disruptive peptides as described before (see Materials and Methods and refs. [7–10, 13]). In these experiments, HEK-293 T cells were co-transfected with receptors separately fused to complementary halves of the yellow fluorescent protein (C-terminal, cYFP, and N-terminal, nYFP), either with MOR-nYFP and MOR-cYFP, Gal_1R-nYFP and Gal_1R-cYFP or MOR-nYFP and Gal_1R-cYFP. Fluorescence was then measured in the absence or presence of synthetic peptides with the amino acid sequence of all TMs of both receptors (TM1 to TM7 of MOR and Gal_1R). These TM peptides were fused to the cell-penetrating HIV transactivator of transcription (TAT) sequence to provide the correct orientation when inserted in the plasma membrane [28]. We could first demonstrate that fluorescence of MOR-nYFP/MOR-cYFP was only reduced in the presence of TM5 and TM6 peptides of MOR (Fig. 2a, upper graph) and fluorescence of Gal_1R-nYFP/Gal_1R-cYFP was reduced by TM5 and TM6 peptides of Gal_1R (Fig. 2b, upper graph), pointing to the involvement of the TM 5/6 interface in the MOR-MOR and Gal_1R-Gal_1R homomers. Notably, when MOR-nYFP and MOR-cYFP were co-transfected with non-fused Gal_1R, fluorescence was only significantly decreased by TM4 and TM5 peptides of MOR (Fig. 2a, lower graph), and when Gal_1R-nYFP and Gal_1R -cYFP were co-transfected with non-fused MOR, fluorescence was decreased by TM4 and TM5 peptides of Gal_1R (Fig. 2b, lower graph). Thus, the interface for both MOR-MOR and Gal_1R-Gal_1R homodimers changed in the presence of the other non-fused receptor from a TM 5/6 to a TM 4/5 interface (Fig. 2a and b). Finally, fluorescence of MOR-nYFP/Gal_1R--nYFP was significantly reduced by TM5 and TM6 peptides of both MOR and Gal_1R (Fig. 2c), pointing to a TM 5/6 interface for the MOR-Gal_1R heteromer. These data reveal TM 5/6 as the most stable interface for MOR-MOR and Gal_1R-Gal_1R homomers, but also for the MOR-Gal_1R heteromeric interface. Significantly, the results suggest a competition for the TM 5/6 interface and indicate an obligatory homodimeric structure of MOR and Gal_1R, for which their interface changes to a less

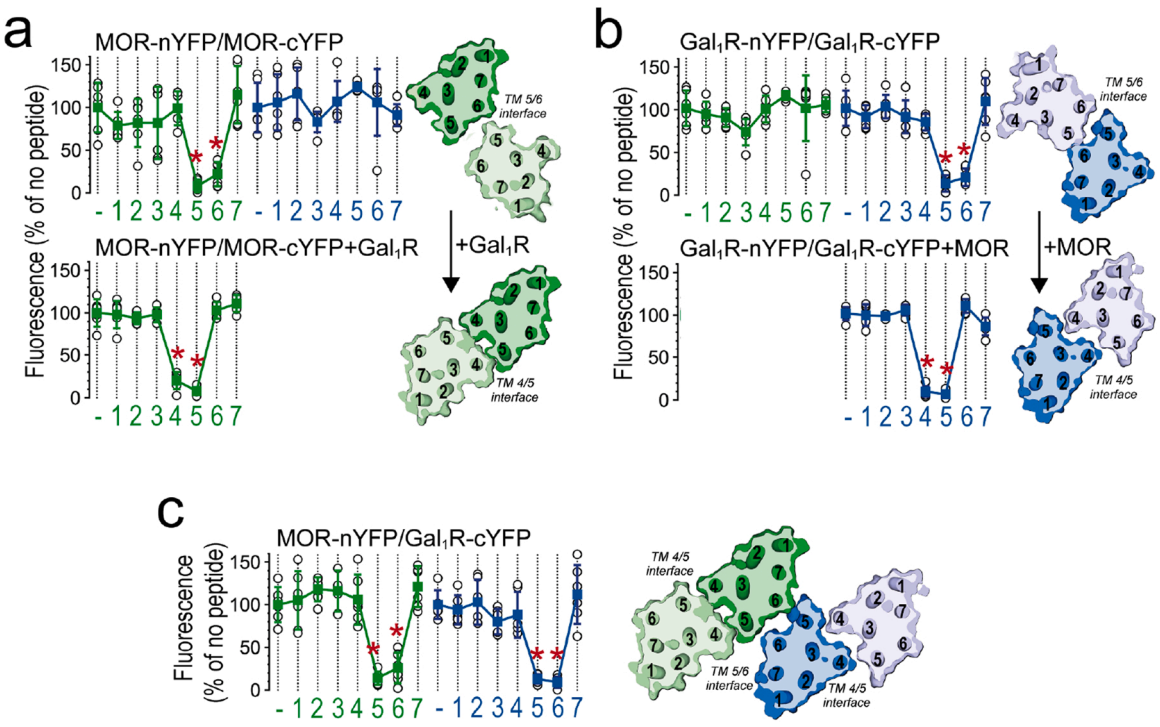

Fig. 2. TM interfaces of MOR and Gal_1R homomers and heteromers in BiFC experiments. Results from BiFC experiments in HEK-293 T cells co-transfected with MOR-nYFP and MOR-cYFP (a), Gal_1R-nYFP and Gal_1R-cYFP (b) or MOR-nYFP and Gal_1R-cYFP (c), in the absence (-) or the presence of the indicated TM peptides (at 4 μM; numbered 1–7) from MOR (green symbols and plots) or Gal_1R (blue symbols and plots), and in the absence or the presence of the co-transfected non-fused Gal_1R or MOR (lower graphs in a and b, respectively); fluorescence values (in means ± S.D.) are expressed as the percentage of the fluorescence in the absence (-) of the indicated TM peptides (n = 6, with triplicates); * represent significantly lower values as compared to control values ($p < 0.001$; one-way ANOVA followed by Dunnett's multiple comparison tests). The schemes in a and b illustrate the corresponding interfaces of the MOR-MOR (a) and Gal_1R-Gal_1R (b) homomers in the absence (upper) and presence (lower) of Gal_1R and MOR, respectively. The scheme in c illustrates the computational model of the MOR-Gal_1R heterotetramer built using the experimental interfaces predicted in panels a–c (TM 5/6 for heterodimerization and TM 4/5 for homodimerization; see text).

favorable TM 4/5 interface in the MOR-Gal_1R heteromer. A sequence analysis of the interactions present in these interfaces is shown in Suppl. Fig. 2. In conclusion, the results indicate the MOR-Gal1R heteromer displays a rhombus-shaped quaternary structure in which homodimerization occurs via the TM 4/5 interface and heteromerization occurs via the TM 5/6 interface (Fig. 2c).

3.3. Single-molecule analysis of the MOR-Gal_1R heteromer reveals a heterotetramer

To determine the preferential number and composition of protomers in the MOR-Gal_1R heteromer, we directly counted the number of protomers assembled at the surface of live HEK-293 T cells by TIRF microscopy photobleaching, as described before [31]. Monomeric teal fluorescent protein 1 (mT) was fused to the C-terminus of Gal_1R and monomeric cherry (mC) to the C-terminus of MOR (mT-Gal_1R and mC-MOR, respectively) to allow for high-resolution, high signal-to-noise TIRF imaging. First, we expressed mT-Gal_1R alone in HEK293T cells and used photobleaching to determine the number of fluorescence-tagged protomers that formed each fluorescent particle. Approximately 75% of the fluorescent particles had two-photobleaching steps, indicating the preferential formation of Gal_1R-Gal_1R homodimers (Fig. 3a and b). The remaining particles were monomeric, and no higher-level oligomers were observed. Similar results (preferential formation of MOR-MOR homodimers) were obtained when mC-MOR was expressed alone (Fig. 3c). Furthermore, we incubated cells with peptides TM4, TM5, TM6 or TM7 of MOR. In agreement with the results obtained with BiFC, TM5 and TM6, but not TM4 or TM7, altered the composition of the fluorescent particles to primarily monomeric, indicating a significant involvement of TM 5 and TM 6 helices in the formation of the MOR-MOR interface. As expected, mT-Gal_1 receptor homodimers were not disrupted following incubation of the cells with these MOR peptides (Fig. 3b).

Next, we studied colocalized fluorescent particles formed when mC-MOR and mT-Gal_1R were expressed together in the same cells (Fig. 3d and e). The majority of the colocalized particles were tetramers composed by two protomers each of MOR and Gal_1R, heteromers of homomers. The selective disruption of these complexes with peptides TM5 and TM6, but not TM4 or TM7, peptides of MOR is in complete agreement with our previous finding with BiFC experiments indicating that the interface of the MOR-Gal_1R heteromer also involves the TM 5 and TM 6 helices of the MOR. Notably, particles studied following incubation of the cells with TM4 of MOR were trimeric, containing a single MOR protomer colocalized with a Gal_1R-Gal_1R homodimer, also confirming the key role for TM 4 in the MOR-MOR homodimer (TM 4/5 interface) of the heterotetramer (Fig. 3e). Finally, we assessed the stoichiometry of mCherry-tagged MOR particles that were not colocalized with Gal_1R in cells co-transfected with mT-Gal_1R and mC-MOR. In agreement with the stoichiometry of isolated mC-MOR (Fig. 3c), these assemblies were primarily dimeric but were disrupted when cells were incubated with TM5 and TM6 but not TM4 or TM7 of MOR (Fig. 3f). The isolated mT-Gal_1Rs also preferentially formed dimers, and as expected these complexes were not disrupted by incubation with TM peptides of MOR (Fig. 3g). Altogether, these data confirm the results from BiFC experiments and demonstrate that, in HEK-293 T co-transfected cells, the MOR-Gal_1R heteromer is a heterotetramer, a heteromer of MOR-MOR and Gal_1R-Gal_1R homomers, in which homodimerization occurs via the TM 4/5 interface and heteromerization occurs via the TM 5/6 interface.

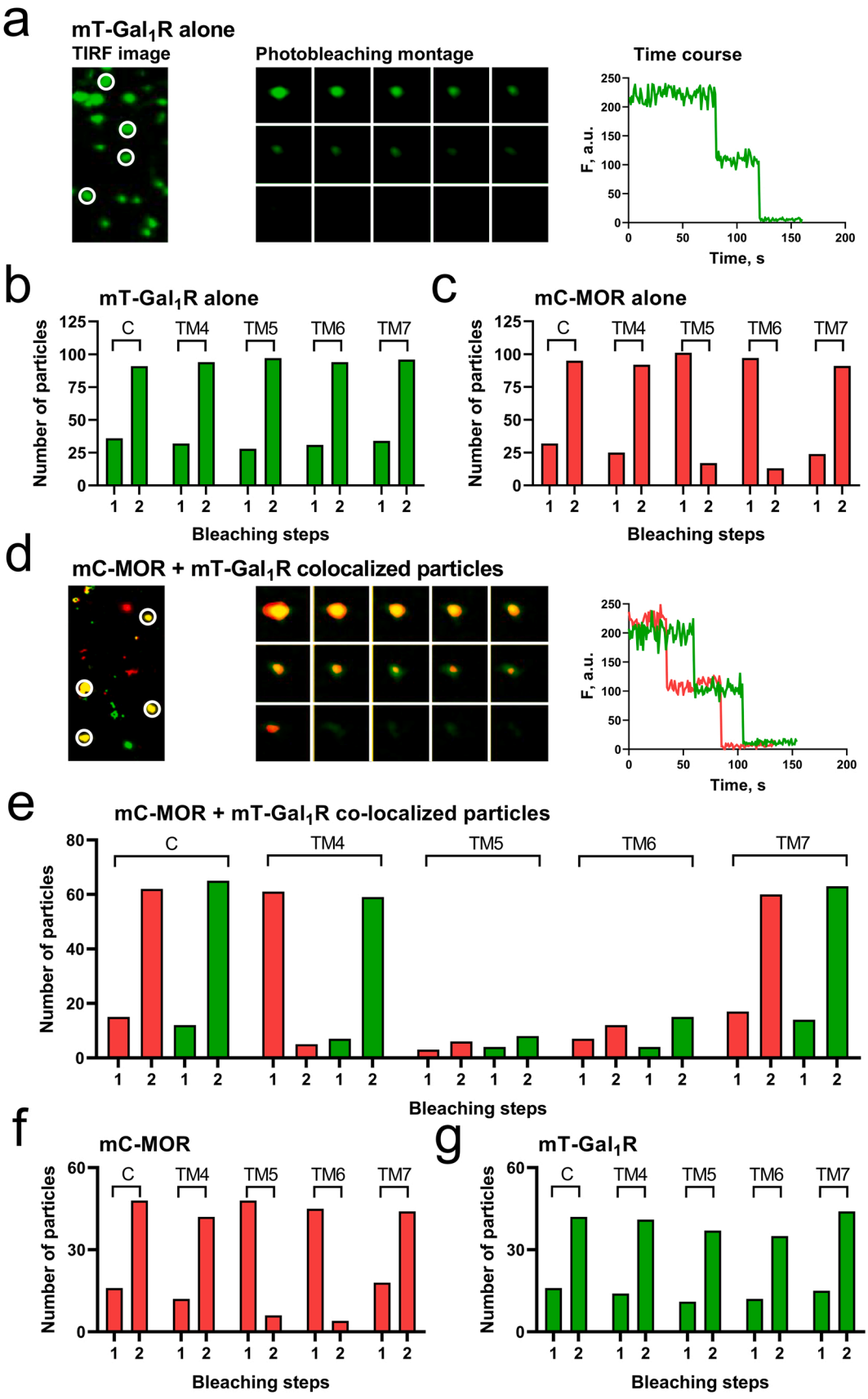

(caption on next page)

Fig. 3. Heterotetrameric structure of the MOR-Gal$_1$R heteromer in TIRF experiments. a. In the left panel, representative TIRF image showing fluorescent particles formed by mT-Gal$_1$R in HEK-293 T cells; in the middle and right panels, example of a single mT-Gal1R particle with the time course for the change in fluorescence intensity (arbitrary units) showing two-step photobleaching. b-c. Results summarizing the number of bleaching steps for mT-Gal$_1$R or mC-MOR expressed separately and studied in the absence (C, control) or presence of the indicated MOR TM peptides (at 1 μM). d. In the left panel, representative TIRF image showing fluorescent particles formed by mT-Gal$_1$R (green), mC-MOR (red) separate and colocalized (yellow); in the middle and right panels, example of a single colocalized particle with the time course for two-photobleaching steps each for mT-Gal$_1$R and mC-MOR, indicating a heterotetramer. e. Result summarizing the composition of colocalized particles studied in the absence (C, control) or presence of the indicated MOR TM peptides (at 1 μM). f-g. Analysis of the non-colocalized mC-MOR and mT-Gal$_1$R particles from cells expressing both receptors studied in the absence (c, control) or presence of the indicated MOR TM peptides (at 1 μM). Data represent particle counts from 4 to 6 cells per condition studied.

3.4. *Promiscuous G protein coupling of Gal$_1$R in the MOR-Gal$_1$R heteromer*

Proximity assessment by BRET is based on the process of transfer of energy from a bioluminescent donor, RLuc, to a fluorescent acceptor chromophore, such as YFP. Fusing RLuc to MOR or Gal$_1$R and mVenus variant of YFP to the α subunit of a G protein, we can analyze the effect of agonists in their ability to change the basal BRET values, as an indirect measure of ligand-induced G protein activation. MOR-RLuc or Gal$_1$R-RLuc and Gi-YFP, Gq-YFP or Gs-YFP constructs were transiently co-transfected to HEK-293 T cells, and concentration-response curves of MOR agonists methadone and fentanyl and Gal$_1$R ligands M617 and M40 were analyzed for EC_{50} and E_{max} values (see Materials and Methods and Fig. 4). As expected from previous studies indicating a selective functional coupling of MOR to Gi/o proteins [15,39], both methadone and fentanyl promoted Gi, but not Gq or Gs, activation (Fig. 4a-c) with no significant differences between their EC_{50} values (Fig. 4d). Also as expected, the Gal$_1$R agonist M617 [22] promoted activation of Gi and no activation of Gs (Fig. 4e, g and h). Less expected was the agonist-like behavior of M40, which has been historically considered and widely used as a non-selective antagonist (see Discussion), produced the same effects as M617 (Fig. 4e, g and h). Additional signaling experiments to confirm that M40 has similar agonist properties than galanin are shown in Suppl. Fig. 4 (see also Fig. 5). Also less expected was that both agonists promoted Gq protein activation (Fig. 4f). Until now it was generally assumed that Gal$_1$R signaling was always regulated in a pertussis toxin-sensitive manner, mediated via Gi/o proteins, while Gal$_2$R was predominantly coupling to Gq proteins (reviewed in ref. [22]). The direction of the concentration-response curves of Gal$_1$R ligands was opposite to that of the MOR ligands. In BRET experiments it is usually expected that ligands induce an increase in BRET values, because of a ligand-induced approximation of the donor and acceptor chromophores [40]. However, RET between two chromophores also depends on their relative orientation (orientation factor or κ^2) [41], which could drive the qualitatively different ligand-induced RET response between the full or complemented RLuc fused to Gal$_1$R and YFP fused to the corresponding Gα.

The CODA-RET assay, a variant of the BRET technique described

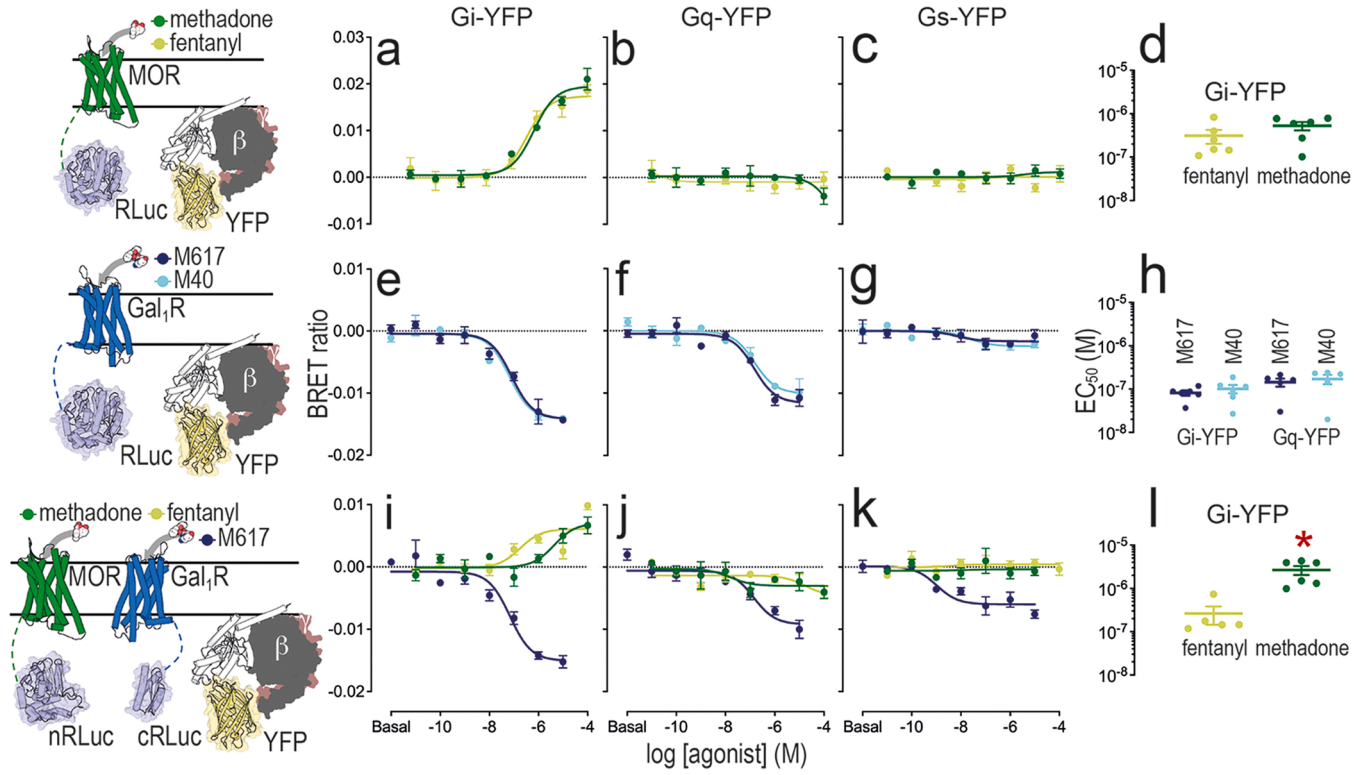

Fig. 4. G protein coupling of MOR, Gal$_1$R and the MOR-Gal$_1$R heteromer in BRET and CODA-RET experiments. a-c. Representative concentration-response curves of methadone (dark green) and fentanyl (light green) of BRET experiments from HEK-293 T cells co-transfected with MOR-RLuc and the α subunit of Gi (a), Gq (b) or Gs (c) fused to YFP. e-g. Representative concentration-response curves of M617 (dark blue) and M40 (light blue) of BRET experiments from HEK-293 T cells co-transfected with Gal$_1$R-RLuc and the α subunit of Gi (e), Gq (f) or Gs (g) fused to YFP. i-k. Representative concentration-response curves of methadone (dark green), fentanyl (light green) and M617 (dark blue) of CODA-RET experiments from HEK-293 T cells co-transfected with MOR-nRLuc, Gal$_1$R-cRLuc and the α subunit of Gi (i), Gq (j) or Gs (k) fused to YFP. d and h. EC_{50} values of the BRET experiments with MOR-RLuc (d) or Gal1R-RLuc (h) (in means ± S.E.M.; n = 6 in all experiments, with triplicates). l. EC_{50} values of the CODA-RET experiments with MOR-nRLuc and Gal$_1$R-cRLuc (n = 5–6, with triplicates). The EC_{50} values of fentanyl and methadone were significantly different in the CODA-RET (*: $p < 0.01$; two-tailed paired *t* test), but not in the BRET experiments.

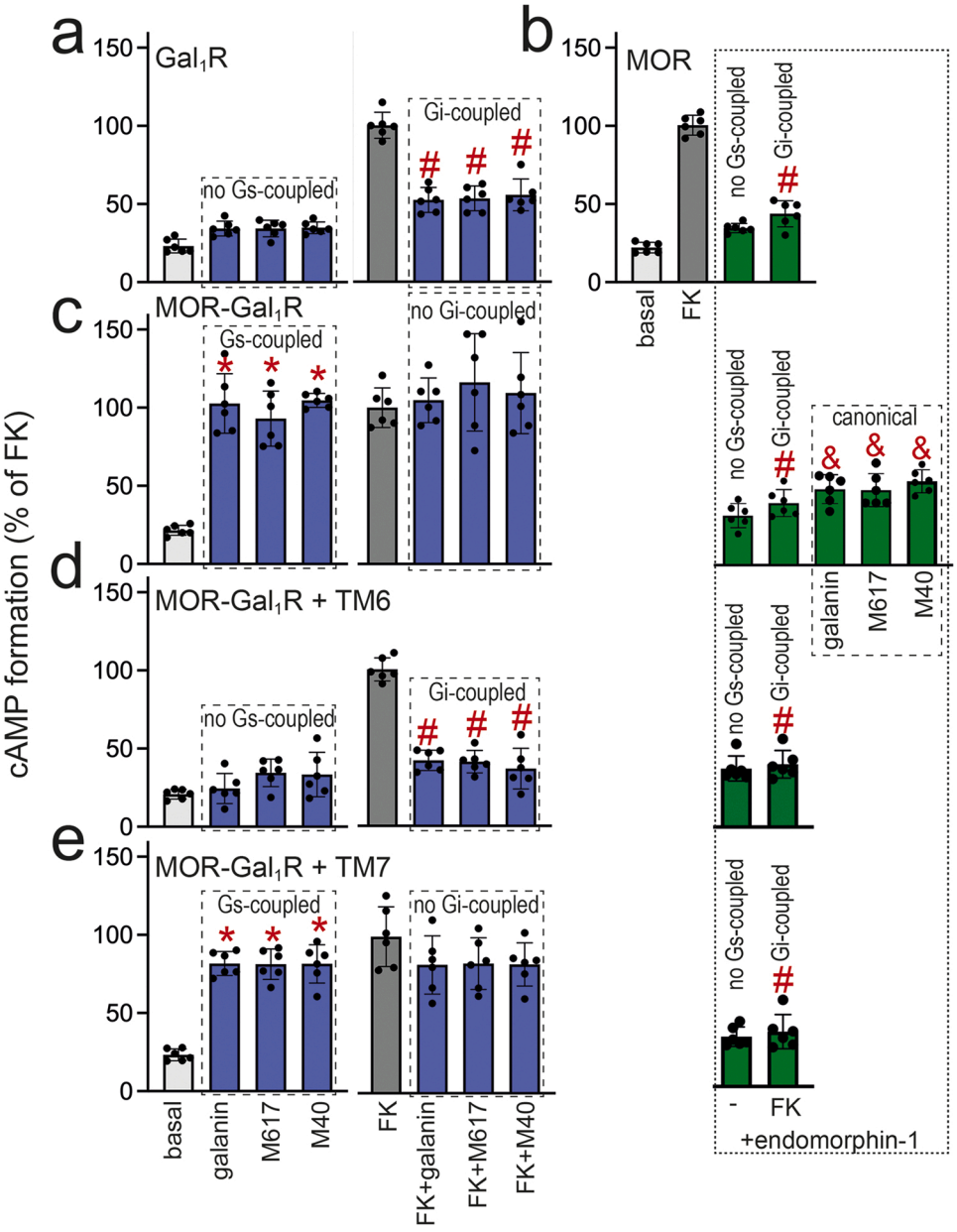

Fig. 5. Preferential Gs protein coupling of Gal_1R when co-expressed with MOR in cAMP formation experiments. Formation of cAMP in HEK-293 T cells transfected with Gal_1R-YFP (a) MOR-RLuc (b) or both (c-e) upon exposure of forskolin (FK; 0.5 μM), galanin ligands (galanin, M617 or M40; all at 0.5 μM; blue bars within dashed frames) and endomorphin-1 (0.5 μM; green bars within dotted frame) alone or combined, in the absence (a-c) and presence (d,e) of the indicated TM peptides (TM6 or TM7; 4 μM) from MOR. "Gs-coupled" or "no-Gs-coupled" indicates the ability to increase or not cAMP formation when administered alone; "Gi-coupled" or "no-Gi-coupled" indicates the ability to decrease or not FK-induced cAMP formation; "canonical" indicates the ability of endomorphin-1 to counteract galanin-, M617- or M40-induced cAMP formation. Values are means ± S.D. (n = 6 with triplicates in all experiments) of the percentage of FK-induced cAMP formation and analyzed statistically with one-way ANOVA, followed by Tukey's multiple comparison test (*: $p < 0.001$, compared with basal; #: $p < 0.001$, compared with FK; &: $p < 0.001$, compared with galanin, M617 or M40 when administered alone).

above, allows the analysis of G protein coupling to a specific GPCR heteromer [42–45]. In this assay, two complementary halves of RLuc (RLuc8 variant; nRLuc and cRLuc) are separately fused to two different GPCR protomers putatively able to dimerize, and YFP is fused to the α subunit of a G protein. Ligand-induced changes in CODA-RET measurements imply a successful complementation of nRluc and cRLuc and, therefore, dimerization of the corresponding protomers. Moreover, it illustrates G protein activation driven by a GPCR heteromer. MOR fused to nRLuc (MOR-nRLuc) and Gal_1R fused to cRLuc (Gal_1R-cRLuc) were co-transfected with Gi-YFP, Gq-YFP or Gs-YFP constructs (Fig. 4i-l). Again, the MOR agonists methadone and fentanyl only promoted activation of Gi (Fig. 4i-k). However, in the MOR-Gal_1R heteromer, the EC_{50} values for methadone were about 10 times higher than for fentanyl (Fig. 4l), which agrees with previous results demonstrating a specific decrease in the potency of methadone in the MOR-Gal_1R heteromer [14]. Remarkably, in the MOR-Gal_1R heteromer, M617 promoted not only Gi and Gq, but also significant Gs activation (with EC_{50} values of 59.0 ± 20.1 nM for Gi, 154.1 ± 25.9 nM for Gq, and 58.7 ± 29.1 nM for Gs) (Fig. 4i-k). Consistent with the results from the BRET assay, the direction of the M617 concentration-response curve was opposite to that of methadone and fentanyl. In summary, the results from the CODA-RET assay indicate Gal_1R is capable of coupling to Gi, Gq and Gs upon heteromerization with MOR.

3.5. *Gs-mediated Gal_1R signaling in cells co-expressing Gal_1R and MOR*

We then investigated the preferred endogenous G protein subtypes coupling to Gal_1R and MOR in HEK-293 T cells transfected with either receptor alone or together. We assessed this by analyzing the effects of agonists on basal and forskolin-induced cAMP formation (Fig. 5a-e). In cells transfected with MOR alone, the endogenous agonist endomorphin-1 (0.5 μM) was unable to modify cAMP levels relative to baseline (Fig. 5b, no Gs-coupled) and significantly decreased forskolin-induced cAMP (Fig. 5b, Gi-coupled). Similarly, in cells expressing Gal_1R alone, galanin, M617 or M40 (each at 0.5 μM) did not modify the basal levels of cAMP (Fig. 5a, no Gs-coupled) and significantly decreased cAMP formation induced by forskolin (Fig. 5a, Gi-coupled). The results obtained with M40 in cAMP measurements confirm its agonist properties (see

above). Thus, both MOR and Gal_1R, when expressed by themselves, signal via their cognate Gi protein. Importantly, a complete signaling switch of Gal_1R was observed in cells co-transfected with both Gal_1R and MOR. In this case, Gal_1R agonists not only failed to decrease forskolin-induced cAMP (Fig. 5c, left panel, no Gi-coupled), but they promoted a significant increase of cAMP formation relative to basal levels (Fig. 5c, left panel, Gs-coupled).

These results strongly suggested that heteromerization with MOR switches the preferential G protein coupling of the Gal_1R from Gi to Gs. By contrast, MOR kept its preferential coupling to Gi proteins in this configuration (Fig. 5c, right panel, no Gs-coupled and Gi-coupled). These data suggest that the MOR-Gal_1R heteromer constitutes an additional example of a Gs-Gi-coupled heterotetramer (see Introduction), with MOR and Gal_1R homodimers coupled to Gi and Gs, respectively, and providing the frame that sustains a canonical Gs-Gi antagonist interaction at the AC level. In agreement, in cells co-transfected with both receptors, MOR agonists inhibited the cAMP-promoting effect of Gal_1R agonists upon simultaneous exposure, revealing the canonical Gs-Gi antagonist interaction (Fig. 5c, right panel, canonical). We next showed that the preferential Gs coupling of the Gal_1R is, in fact, a property of the MOR-Gal_1R heteromer. In the presence of the TM6 peptide of MOR, which disrupts the heteromeric interface, Gal_1R agonists switched from inducing cAMP production (Gs-coupled) back to inhibiting forskolin-induced cAMP formation (Gi-coupled) (Fig. 5e, left panel). In contrast, incubation with the TM7 peptide of MOR, which does not disrupt heteromer formation, had no such effect. The MOR agonist endomorphin-1 remained Gi-coupled in the presence of these peptides (Fig. 5d and e, right panels).

3.6. *The G protein subtype coupling to Gal_1R depends on its homomeric interface*

To elucidate the molecular mechanism underlying the preferential Gs coupling of Gal_1R in the MOR-Gal_1R heteromer, we constructed

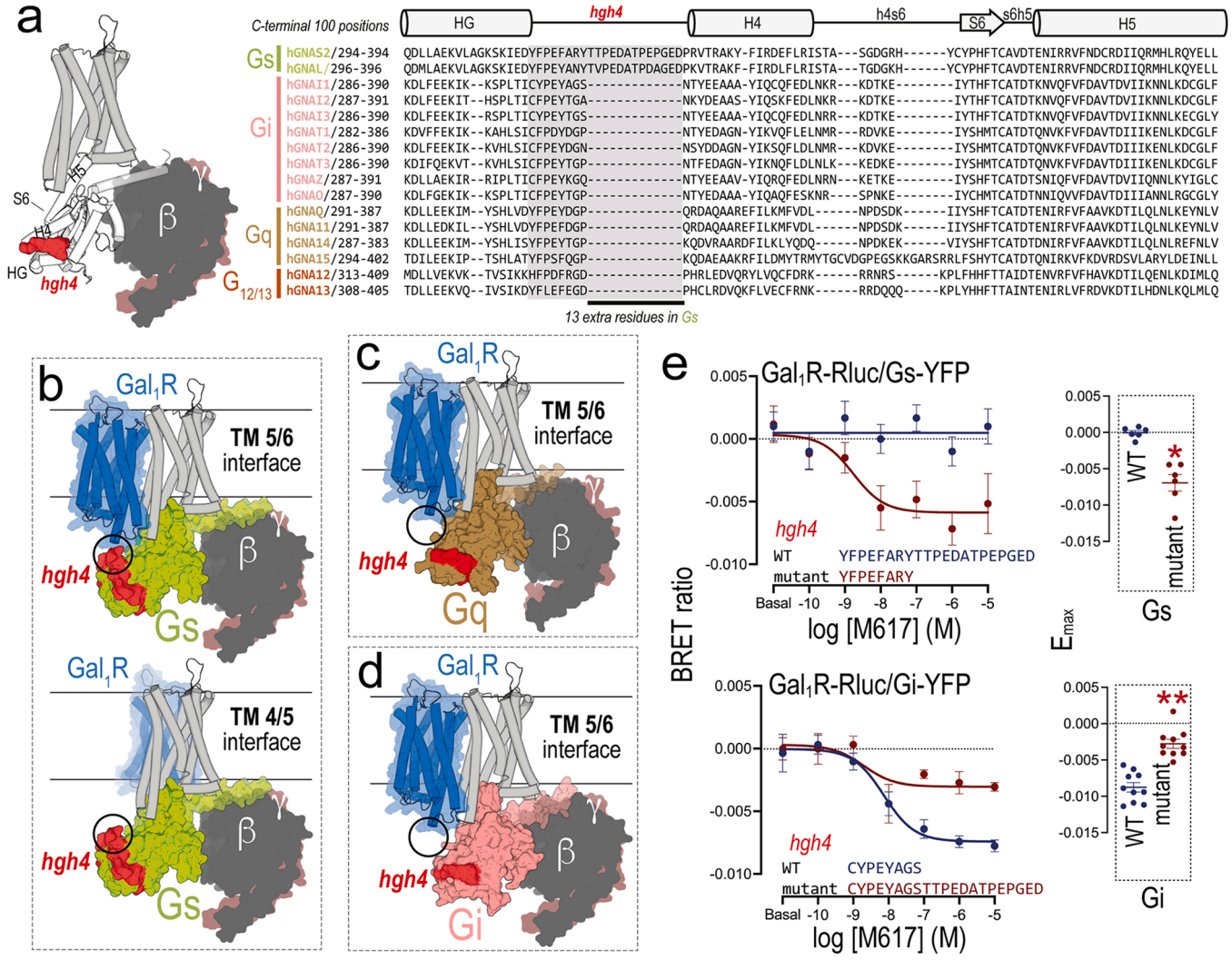

Fig. 6. Dimeric interface-dependent hindering role of the *hgh4* loop of the Gαs subunit in its ability to couple to Gal_1R. a. Sequence alignment of the C-terminal 100 amino acids of the sixteen Gα subunits, as described in GproteinDb [59]. The 13 extra residues of the *hgh4* loop (in red), between HG and H4 helices of the Gαs subunits (see scheme on the left panel), that are absent in the other G protein subtypes, are highlighted in grey. b-d. Computational models of the Gal_1R-Gal_1R homodimer, constructed using the TM 5/6 interface (b, upper panel; c; d) or the TM 4/5 (b, lower panel) interface, in complex with Gs (b), Gi (c), and Gq (d). The encircled area shows the clash of the 13 extra residues of Gs with the G protein unbound protomer in the TM 5/6 interface. e. Representative concentration-response curves of the M617 agonist of BRET experiments from HEK-293 T cells co-transfected with Gal_1R-RLuc and WT Gs fused to YFP (blue line; left panel) or a mutant Gαs (with the extra 13 residues being removed) fused to YFP (red curve; left panel); or cells co-transfected with Gal_1R-RLuc and WT Gi fused to YFP (blue curve; middle panel) or a mutant Gαi (with the extra 13 residues being added) fused to YFP (red curve; middle panel). In the right panel (e), comparison of E_{max} values of the BRET experiments between WT and mutant α-subunits (in means ± S.E.M.; n = 6 in all experiments, with triplicates). The E_{max} values between WT and mutant α-subunits were significantly different (*: $p < 0.05$, **: $p < 0.01$; two-tailed paired *t* test).

computational models of Gal_1R-Gal_1R homodimers, built via the TM 4/5 and TM 5/6 interfaces, bound to Gi, Gs, and Gq (see Materials and Methods) (Fig. 6). Sequence alignment of C-terminal residues of the sixteen Gα subunits revealed a specific sequence of 13 extra Gs residues that is absent in the other G protein subtypes (Fig. 6a). These extra residues are localized in the *hgh4* loop, between HG and H4 helices, in the α-helical domain of the G protein. Noticeably, in the model, the additional length of *hgh4* of Gs clashes with the G protein unbound Gal_1R protomer in the TM 5/6 interface (Fig. 6b, upper panel) but it is tolerated in the TM 4/5 interface (Fig. 6b, lower panel). The shorter *hgh4* loop of Gi (Fig. 6c), Gq (Fig. 6d) or Go (not shown) permits their binding to the Gal_1R-Gal_1R homodimer in the TM 5/6 interface. To experimentally validate this hypothesis, we created a mutant Gs in which these extra 13 residues were removed and a mutant Gi in which these residues were added in the corresponding *hgh4* locus (see Materials and Methods). Both mutants were fused to YFP and used in BRET experiments in cells co-transfected with Gal_1R-RLuc, in the absence of MOR, and either the mutant Gs-YFP or the mutant Gi-YFP or the corresponding wild-type (WT) constructs (Fig. 6e). As predicted, the Gal_1R agonist M617 activated the mutant Gs (with short *hgh4*), since it could bind to the TM 5/6 interface (due to the absence of MOR) of the Gal_1R-Gal_1R homodimer, while M617 promoted a much weaker activation of mutant Gi as compared to WT Gi (with long and short *hgh4*, respectively), since it could not properly bind to the TM 5/6 interface of the Gal_1R-Gal_1R homodimer. These computational and experimental results indicate that the ability of Gs to couple to the Gal_1R-Gal_1R homodimer is determined by the change in its homomeric interface induced by heteromerization with MOR.

4. Discussion

The present study reports converging evidence, using different methodologies, for a predominant homodimeric structure of both MOR and Gal_1R, and for their preference to form functional heterotetramers coupled to Gs and Gi proteins that antagonistically interact at the level of the effector AC. The results therefore support the previously hypothesized view of the GPCR heterotetramer composed of two different GPCR homodimers respectively coupled to Gs and Gi proteins and AC as a common functional macromolecular complex [11], more recently conceptualized as a G protein-coupled receptor-effector macromolecular membrane assembly (GEMMA) [46].

Using a TM-peptide-interfering approach combined with biophysical and biochemical techniques (BiFC assays and TIRF microscopy and cAMP measurements), we could propose the TM 5/6 MOR-Gal_1R heteromeric interface, which was the same as the preferred homomeric interface of MOR and Gal_1R homodimers when each receptor was expressed alone. Yet, when forming heteromers, MOR and Gal_1R still preferred a homodimeric to the monomeric structure, although with a less preferred TM 4/5 homomeric interface. Importantly, this heteromerization-induced change in the homomeric interface had a significant functional consequence: a switch in the G protein coupling of Gal_1R, from Gi to Gs, without modifying the G protein preference of the MOR. Previous studies with other GPCRs reported changes in their functional properties when heteromerizing. For instance, the switch is observed in G-protein coupling of serotonin 5-HT_{2A} receptor from Gq to Gi proteins upon heteromerization with the cannabinoid CB_1 receptor [47] or the disappearance of the pronounced constitutive activity of the adenosine A_{2A} receptor when forming heteromers with the adenosine A_1 receptor or the dopamine D_2 receptor, but not with the cannabinoid CB_1 receptor [9]. However, to our knowledge, this is the first study to unveil the molecular mechanism behind a heteromerization-dependent change in GPCR function, which we demonstrate is a facilitation of Gs coupling upon a switch in the Gal_1R homomeric interface.

Although most recent studies addressing the question of oligomerization of MOR using single molecule techniques support its predominant monomeric structure [20,22], our study showed preferential formation of MOR dimers when the mC-tagged subunit was expressed alone in HEK293 cells (Fig. 3). This discrepancy in the reported oligomerization state of MOR might reflect differences in the experimental approach. Specifically, Möller et al. [20] employed single particle tracking algorithms to follow the trajectory of receptors 4–6 h post transfection with SNAP-tagged subunits with the goal of studying receptors at low density at the plasma membrane. Asher and colleagues [21] inferred stoichiometry from single molecule FRET studies. Here, we employed photobleaching of C-terminal fluorescent tagged subunits 24 h after transfection to assess stoichiometry directly by counting the number of subunits in each GPCR complex. This approach has been used extensively to assess the stoichiometry of membrane-motors and ion channel complexes at the surface of transfected cells and corresponds well with real-time measures of protein function made in the same cells [42,48–50]. Although organic dyes, such as SNAP-tags, typically have a higher quantum yield and photostability than fluorescent proteins, the chemical efficiency of labeling in live cells is variable. In contrast, fluorescent proteins are present on each expressed subunit in a complex, excluding those fluorophores that are potentially pre-bleached or that have adopted a non-excitable configuration. However, if anything, these caveats bias datasets towards a lower stoichiometry [51]. Therefore, our results show that MOR forms stable dimers but not higher order complexes. Similarly, we observed that Gal_1R receptors tagged with mT preferentially form dimers rather than monomers, and do not form higher order complexes. Importantly, the results of TIRF experiments in cells co-expressing MOR and Gal_1R were in complete agreement with the observations from the BiFC experiments. Of particular note were the results obtained with TM4 of the MOR, which promoted the predominant formation of trimeric fluorescent particles, composed of one MOR with two Gal_1R. On the other hand, TM4 of the MOR did not disrupt MOR homodimerization when transfected alone, in agreement with the fourth TM domain of MOR being required at the MOR-MOR interface only in the context of the heterotetramers. As expected, both TM5 and TM6 of the MOR disrupted the formation of heterotetramers.

The converging evidence for MOR-MOR homodimerization obtained by using different methodologies was further confirmed by the results of radioligand-binding experiments. In fact, there is already significant support in the literature indicating that classical radioligand binding experiments can provide a valid methodology to study GPCR oligomerization in most experimental settings, including native tissues [1,6,36,37]. The present study offers an important example of the validity of radioligand binding techniques for the demonstration and analysis of GPCR oligomers with the application of the 'dimer receptor model' [27].

Apart from the general conceptual importance for the field of GPCR oligomerization, studies with the MOR-Gal_1R heteromer have already shown to have important translational implications in the fields of opioid analgesia and opioid use disorder. The MOR-Gal_1R heteromer localized in the VTA is involved in the dopaminergic effects of opioids and provides a pharmacodynamic explanation for the weaker dopaminergic and euphoric properties of methadone [14]. Work is in progress to determine the mechanism underlying this specific insensitivity of the MOR-Gal_1R heteromer to methadone, which should provide clues for finding additional molecules that poorly bind or activate the MOR in the VTA while preserving significant activity for MOR in other nervous system regions that mediate analgesia.

In the previous studies on the MOR-Gal_1R heteromer, we provided in vitro evidence in mammalian transfected cells and in situ and in vivo evidence in the rat VTA for a heteromer-dependent allosteric interaction by which Gal_1R ligands decrease the affinity of MOR ligands and antagonize MOR-mediated G protein activation, signaling and dopaminergic activation [13,14]. Therefore, development of small molecule agonists that target the Gal_1R in the MOR-Gal_1R heteromer represents a promising approach to counteract the unwanted dopaminergic effects of opioids while preserving or even potentiating their analgesic effects at the spinal level, as previously described [52]. The currently available selective Gal_1R agonists, such as M617 and M40 are large peptides that

cannot be orally or systemically administered to reach the CNS. An unexpected additional result of the present study was the finding of agonist activity of M40, since it has been generally considered as a canonical non-selective galanin receptor antagonist. For example, M40 blocks feeding, scopolamine-induced acetylcholine release, and anticonvulsant activity induced by central galanin administration [22, 53–55]. Nevertheless, M40 has been reported to have agonist-like activity under some conditions, where it mimics the effects of galanin by attenuating forskolin-induced formation of cAMP, suppressing glutamate release, and activating inwardly rectifying potassium conductance [56–58]. While the mechanistic reasons for these disparate findings are not clear, they highlight that care must be taken to characterize the valence of galanin receptor ligands in each specific system.

The present study adds a new unforeseen property of the MOR-Gal_1R heteromer, its specific ability to promote Gs coupling to the Gal_1R. One limitation of the current study is that experiments were performed exclusively in vitro, in mammalian transfected cells. If the tetrameric structure of the MOR-Gal_1R heteromer represents a significant population of both receptors in the VTA, or other brain areas, we should expect that in those neuroanatomical substrates the effects of galanin or other Gal_1R agonists are dependent on the activation of the canonical Gs-cAMP-protein kinase A signaling. Contrary to the allosteric interaction by which Gal_1R ligands antagonize MOR signaling, this effect would be counteracted by MOR-mediated signaling, via a canonical Gs-Gi antagonistic interaction at the AC level. Experiments are in progress to establish the predominant heterotetrameric structure of MOR-Gal_1R heterotetramer in the brain, as well as its pharmacological significance.

CRediT authorship contribution statement

Paulo A. De Oliveira, Estefanía Moreno, Nil Casajuana-Martin, Verònica Casadó-Anguera, Ning-Sheng Cai, Gisela Andrea Camacho-Hernandez, Hu Zhu, Alessandro Bonifazi, Matthew D. Hall, David Weinshenker, Amy Hauck Newman, Diomedes E. Logothetis, Vicent Casadó, Leigh D. Plant, Leonardo Pardo and Sergi Ferré conceived the experiments. Paulo A. De Oliveira, Estefanía Moreno, Nil Casajuana-Martin, Verònica Casadó-Anguera, Ning-Sheng Cai, Gisela Andrea Camacho-Hernandez, Hu Zhu and Leigh D. Plant performed the experiments. Paulo A. De Oliveira, Estefanía Moreno, Nil Casajuana-Martin, Verònica Casadó-Anguera, Ning-Sheng Cai, Gisela Andrea Camacho-Hernandez, Hu Zhu, David Weinshenker, Vicent Casadó, Leigh D. Plant, Leonardo Pardo and Sergi Ferré wrote the paper. Sergi Ferré and Leonardo Pardo initiated the project.

Declaration of Competing Interest

The authors declare no competing interests.

Data availability

All data needed to evaluate the conclusions in the paper are present in the paper or the Supplementary materials.

Acknowledgements

We are grateful to Aishwarya Chandrashekar for technical support with TIRF microscopy, the late R.Y. Tsien (UCSD) for the mCherry clone and A. Periasamy (University of Virginia) for mTFP1. Funding: National Institute on Drug Abuse, USA, intramural research funds (P.A.D.O., N.-S. C., G.A.C.-H., A.B., A.H.N., S.F.); National Center for Advancing Translational Sciences, USA (NCATS) (H.Z., M.D.H.); Trans-NIH HEAL Initiative, USA (the NIH HEAL Initiative Data policy is available at: https://heal.nih.gov/about/public-access-data") (P.A.D.O., H.Z., M.D.H.); 'Ministerio de Ciencia e Innovación/Agencia Estatal de Investigación' (MCIN/AEI) and FEDER, Spain, grant SAF2017–87629-R (E.M., V.C.-A., V.C.); MCIN/AEI, grants 10.13039/501100011033 and PID2020–113938RB-I00 (E.M, V.C.-A, V.C.); Juan de la Cierva fellowship, Spain, grant FJC2019-I (V.C.-A.); "Generalitat de Catalunya", Spain, grant 2017-SGR-1497 (E.M., V.C.-A., V.C.); MCIN/AEI, grant PID2019–109240RB-I00 (NCM, LP); National Institutes of Health, USA, grants R01DA049257 (D.W.) and R01HL144615 (L.D.P.).

Appendix A. Supporting information

Supplementary data associated with this article can be found in the online version at doi:10.1016/j.phrs.2022.106322.

References

[1] S. Ferré, V. Casadó, L.A. Devi, M. Filizola, R. Jockers, M.J. Lohse, G. Milligan, J. P. Pin, X. Guitart, G protein-coupled receptor oligomerization revisited: functional and pharmacological perspectives, *Pharmacol. Rev.* 66 (2014) 413–434.
[2] I. Gomes, M.A. Ayoub, W. Fujita, W.C. Jaeger, K.D. Pfleger, L.A. Devi, G protein-coupled receptor heteromers, Annu. Rev. Pharmacol. Toxicol. 56 (2016) 403–425.
[3] S.A. Gaitonde, J. González-Maeso, Contribution of heteromerization to G protein-coupled receptor function, *Curr. Opin. Pharmacol.* 32 (2017) 23–31.
[4] W.B. Asher, S. Mathiasen, M.D. Holsey, S.G. Grinnell, N.A. Lambert, J.A. Javitch, Extreme vetting of dopamine receptor oligomerization, in: K. Herrick-Davis, G. Milligan, G. Di Giovanni (Eds.), G-Protein-Coupled Receptor Dimers, Springer, Switzerland, 2017, pp. 99–127.
[5] V.V. Gurevich, E.V. Gurevich, GPCRs and signal transducers: interaction stoichiometry, Trends Pharmacol. Sci. 39 (2018) 672–684.
[6] S. Ferré, F. Ciruela, V. Casadó, L. Pardo L, Oligomerization of G protein-coupled receptors: Still doubted? Prog. Mol. Biol. Transl. Sci. 169 (2020) 297–321.
[7] G. Navarro, A. Cordomí, V. Casadó-Anguera, E. Moreno, N.S. Cai, A. Cortés, E. I. Canela, C.W. Dessauer, V. Casadó, L. Pardo, C. Lluís, S. Ferré, Evidence for functional pre-coupled complexes of receptor heteromers and adenylyl cyclase, *Nat. Commun.* 9 (2018) 1242.
[8] G. Navarro, A. Cordomí, M. Brugarolas, E. Moreno, D. Aguinaga, L. Pérez-Benito, S. Ferre, A. Cortés, V. Casadó, J. Mallol, E.I. Canela, C. Lluís, L. Pardo, P. J. McCormick, R. Franco, Cross-communication between G_i and G_s in a G-protein-coupled receptor heterotetramer guided by a receptor C-terminal domain, BMC Biol. 16 (2018) 24.
[9] A. Köfalvi, E. Moreno, A. Cordomí, N.S. Cai, V. Fernández-Dueñas, S.G. Ferreira, R. Guixà-González, M. Sánchez-Soto, H. Yano, V. Casadó-Anguera, R.A. Cunha, A. M. Sebastião, F. Ciruela, L. Pardo, V. Casadó, S. Ferré, Control of glutamate release by complexes of adenosine and cannabinoid receptors, BMC Biol. 18 (2020) 9.
[10] R. Franco, A. Cordomí, C. Llinas Del Torrent, A. Lillo, J. Serrano-Marín, G. Navarro, L. Pardo, Structure and function of adenosine receptor heteromers, *Cell. Mol. Life Sci.* 78 (2021) 3957–3968.
[11] S. Ferré, The GPCR heterotetramer: challenging classical pharmacology, *Trends Pharmacol. Sci.* 36 (2015) 145–152.
[12] C. Qi, S. Sorrentino, O. Medalia, V.M. Korkhov, The structure of a membrane adenylyl cyclase bound to an activated stimulatory G protein, Science 364 (2019) 389–394.
[13] E. Moreno, C. Quiroz, W. Rea, N.S. Cai, J. Mallol, A. Cortés, C. Lluís, E.I. Canela, V. Casadó, S. Ferré, Functional μ-Opioid-Galanin Receptor Heteromers in the Ventral Tegmental Area, *J. Neurosci.* 37 (2017) 1176–1186.
[14] N.S. Cai, C. Quiroz, J. Bonaventura, A. Bonifazi, T.O. Cole, J. Purks, A.S. Billing, E. Massey, M. Wagner, E.D. Wish, X. Guitart, W. Rea, S. Lam, E. Moreno, V. Casadó-Anguera, A.D. Greenblatt, A.R. Jacobson, K.C. Rice, V. Casadó, A.H. Newman, J. W. Winkelman, M. Michaelides, E. Weintraub, N.D. Volkow, A.M. Belcher, S. Ferré, Opioid-galanin receptor heteromers mediate the dopaminergic effects of opioids, J. Clin. Invest 129 (2019) 2730–2744.
[15] T. Che, B.L. Roth, Structural insights accelerate the discovery of opioid alternatives, Annu. Rev. Biochem. 90 (2021) 739–761.
[16] D. Wang, X. Sun, L.M. Bohn, W. Sadée, Opioid receptor homo- and heterodimerization in living cells by quantitative bioluminescence resonance energy transfer, *Mol. Pharmacol.* 67 (2005) 2173–2184.
[17] U. Golebiewska, J.M. Johnston, L. Devi, M. Filizola, S. Scarlata, Differential response to morphine of the oligomeric state of μ-opioid in the presence of δ-opioid receptors, Biochemistry 50 (2011) 2829–2837.
[18] A. Manglik, A.C. Kruse, T.S. Kobilka, F.S. Thian, J.M. Mathiesen, R.K. Sunahara, L. Pardo, W.I. Weis, B.K. Kobilka, S. Granier, Crystal structure of the μ-opioid receptor bound to a morphinan antagonist, Nature 485 (2012) 321–326.
[19] D. Meral, D. Provasi, D. Prada-Gracia, J. Möller, K. Marino, M.J. Lohse, M. Filizola, Molecular details of dimerization kinetics reveal negligible populations of transient μ-opioid receptor homodimers at physiological concentrations, *Sci. Rep.* 8 (2018) 7705.
[20] J. Möller, A. Isbilir, T. Sungkaworn, B. Osberg, C. Karathanasis, V. Sunkara, E. O. Grushevskyi, A. Bock, P. Annibale, M. Heilemann, C. Schütte, M.J. Lohse, Single-molecule analysis reveals agonist-specific dimer formation of μ-opioid receptors, *Nat. Chem. Biol.* 16 (2020) 946–954.
[21] W.B. Asher, P. Geggier, M.D. Holsey, G.T. Gilmore, A.K. Pati, J. Meszaros, D. S. Terry, S. Mathiasen, M.J. Kaliszewski, M.D. McCauley, A. Govindaraju, Z. Zhou, K.G. Harikumar, K. Jaqaman, L.J. Miller, A.W. Smith, S.C. Blanchard, J.A. Javitch, Single-molecule FRET imaging of GPCR dimers in living cells, Nat. Methods 18 (2021) 397–405.

[22] R. Lang, A.L. Gundlach, F.E. Holmes, S.A. Hobson, D. Wynick, T. Hökfelt, B. Kofler, Physiology, signaling, and pharmacology of galanin peptides and receptors: three decades of emerging diversity, *Pharmacol. Rev.* 67 (2015) 118–175.
[23] J. Duan, D.D. Shen, T. Zhao, S. Guo, X. He, W. Yin, P. Xu, Y. Ji, L.N. Chen, J. Liu, H. Zhang, Q. Liu, Y. Shi, X. Cheng, H. Jiang, X.H. Eric, Y. Zhang, X. Xie, Y. Jiang, Molecular basis for allosteric agonism and G protein subtype selectivity of galanin receptors, Nat. Commun. 13 (2022) 1364.
[24] S.A. Wirz, C.N. Davis, X. Lu, T. Zal, T. Bartfai, Homodimerization and internalization of galanin type 1 receptor in living CHO cells, Neuropeptides 39 (2005) 535–546.
[25] K. Fuxe, D.O. Borroto-Escuela, W. Romero-Fernandez, A.O. Tarakanov, F. Calvo, P. Garriga, M. Tena, M. Narvaez, C. Millón, C. Parrado, F. Ciruela, L.F. Agnati, J. A. Narvaez, Z. Díaz-Cabiale, On the existence and function of galanin receptor heteromers in the central nervous system, Front. Endocrinol. 3 (2012) 127.
[26] V. Casadó, A. Cortés, F. Ciruela, J. Mallol, S. Ferré, C. Lluis, E.I. Canela, R. Franco, Old and new ways to calculate the affinity of agonists and antagonists interacting with G-protein-coupled monomeric and dimeric receptors: the receptor-dimer cooperativity index, *Pharmacol. Ther.* 116 (2007) 343–354.
[27] V. Casadó, A. Cortés, J. Mallol, K. Pérez-Capote, S. Ferré, C. Lluis, R. Franco, E. I. Canela, GPCR homomers and heteromers: a better choice as targets for drug development than GPCR monomers? *Pharmacol. Ther.* 124 (2009) 248–257.
[28] S.Q. He, Z.N. Zhang, J.S. Guan, H.R. Liu, B. Zhao, H.B. Wang, Q. Li, H. Yang, J. Luo, Z.Y. Li, Q. Wang, Y.J. Lu, L. Bao, X. Zhang, Facilitation of μ-opioid receptor activity by preventing δ-opioid receptor-mediated codegradation, Neuron 69 (2011) 120–131.
[29] S.R. Schwarze, A. Ho, A. Vocero-Akbani, S.F. Dowdy, In vivo protein transduction: delivery of a biologically active protein into the mouse, Science 285 (1999) 1569–1572.
[30] M.H. Ulbrich, E.Y. Isacoff, Subunit counting in membrane-bound proteins, Nat. Meth 4 (2007) 319–321.
[31] L.D. Plant, D. Xiong, H. Dai, S.A. Goldstein, Individual IKs channels at the surface of mammalian cells contain two KCNE1 accessory subunits, Proc. Natl. Acad. Sci. USA 111 (2014) E1438–E1446.
[32] J. Huang, S. Chen, J.J. Zhang, X.Y. Huang, Crystal structure of oligomeric beta1-adrenergic G protein-coupled receptors in ligand-free basal state, Nat. Struct. Mol. Biol. 20 (2013) 419–425.
[33] A. Koehl, H. Hu, S. Maeda, Y. Zhang, Q. Qu, J.M. Paggi, N.R. Latorraca, D. Hilger, R. Dawson, H. Matile, G. Schertler, S. Granier, W.I. Weis, R.O. Dror, A. Manglik, G. Skiniotis, B.K. Kobilka, Structure of the micro-opioid receptor-Gi protein complex, Nature 558 (2018) 547–552.
[34] Q. Liu, D. Yang, Y. Zhuang, T.I. Croll, X. Cai, A. Dai, X. He, J. Duan, W. Yin, C. Ye, F. Zhou, B. Wu, Q. Zhao, H.E. Xu, M.W. Wang, Y. Jiang, Ligand recognition and G-protein coupling selectivity of cholecystokinin A receptor, *Nat. Chem. Biol.* 17 (2021) 1238–1244.
[35] M.A. Martí-Renom, A.C. Stuart, A. Fiser, R. Sánchez, F. Melo, A. Sali, Comparative protein structure modeling of genes and genomes, Annu. Rev. Biophys. Biomol. Struct. 29 (2000) 291–325.
[36] D.S. Redka, H. Heerklotz, J.W. Wells, Efficacy as an intrinsic property of the M(2) muscarinic receptor in its tetrameric state, Biochemistry 52 (2013) 7405–7427.
[37] D.S. Redka, T. Morizumi, G. Elmslie, P. Paranthaman, R.V. Shivnaraine, J. Ellis, O. P. Ernst, J.W. Wells, Coupling of g proteins to reconstituted monomers and tetramers of the M2 muscarinic receptor, *J. Biol. Chem.* 289 (2014) 24347–24365.
[38] V. Casadó-Anguera, E. Moreno, J. Mallol, S. Ferré, E.I. Canela, A. Cortés, V. Casadó, Reinterpreting anomalous competitive binding experiments within G protein-coupled receptor homodimers using a dimer receptor model, Pharmacol. Res. 139 (2019) 337–347.
[39] J.T. Williams, S.L. Ingram, G. Henderson, C. Chavkin, M. von Zastrow, S. Schulz, T. Koch, C.J. Evans, M.J. Christie, Regulation of μ-opioid receptors: desensitization, phosphorylation, internalization, and tolerance, *Pharmacol. Rev.* 65 (2013) 223–254.
[40] C. Galés, J.J. Van Durm, S. Schaak, S. Pontier, Y. Percherancier, M. Audet, H. Paris, M. Bouvier, Probing the activation-promoted structural rearrangements in preassembled receptor-G protein complexes, *Nat. Struct. Mol. Biol.* 13 (2006) 778–786.
[41] S.M. Müller, H. Galliardt, J. Schneider, B.G. Barisas, T. Seidel, Quantification of Förster resonance energy transfer by monitoring sensitized emission in living plant cells, *Front. Plant Sci.* 4 (2013) 413.
[42] X. Guitart, G. Navarro, E. Moreno, H. Yano, N.S. Cai, M. Sánchez-Soto, S. Kumar-Barodia, Y.T. Naidu, J. Mallol, A. Cortés, C. Lluís, E.I. Canela, V. Casadó, P. J. McCormick, S. Ferré, Functional selectivity of allosteric interactions within G protein-coupled receptor oligomers: the dopamine D1-D3 receptor heterotetramer, *Mol. Pharmacol.* 86 (2014) 417–429.
[43] J. Bonaventura, G. Navarro, V. Casadó-Anguera, K. Azdad, W. Rea, E. Moreno, M. Brugarolas, J. Mallol, E.I. Canela, C. Lluís, A. Cortés, N.D. Volkow, S. N. Schiffmann, S. Ferré, V. Casadó, Allosteric interactions between agonists and antagonists within the adenosine A2A receptor-dopamine D2 receptor heterotetramer, Proc. Natl. Acad. Sci. USA 112 (2015) E3609–E3618.
[44] E. Urizar, H. Yano, R. Kolster, C. Galés, N. Lambert, J.A. Javitch, CODA-RET reveals functional selectivity as a result of GPCR heteromerization, *Nat. Chem. Biol.* 7 (2011) 624–630.
[45] V. Casadó-Anguera, E. Moreno, M. Sánchez-Soto, N.S. Cai, J. Bonaventura, P. Homar-Ruano, M. Rubinstein, A. Cortés, E.I. Canela, S. Ferré, V. Casadó, Heteromerization between α_{2A} adrenoceptors and different polymorphic variants of the dopamine D_4 receptor determines pharmacological and functional differences. Implications for impulsive-control disorders, *Pharmacol. Res.* 170 (2021), 105745.
[46] S. Ferré, F. Ciruela, C.W. Dessauer, J. González-Maeso, T.E. Hébert, R. Jockers, D. E. Logothetis, L. Pardo, G protein-coupled receptor-effector macromolecular membrane assemblies (GEMMAs), *Pharmacol. Ther.* 231 (2022), 107977.
[47] X. Viñals, E. Moreno, L. Lanfumey, A. Cordomí, A. Pastor, R. de La Torre, P. Gasperini, G. Navarro, L.A. Howell, L. Pardo, C. Lluís, E.I. Canela, P. J. McCormick, R. Maldonado, P. Robledo, Cognitive Impairment Induced by Delta9-tetrahydrocannabinol Occurs through Heteromers between Cannabinoid CB1 and Serotonin 5-HT2A Receptors, PLoS Biol. 13 (2015), e1002194.
[48] M.C. Leake, J.H. Chandler, G.H. Wadhams, F. Bai, R.M. Berry, J.P. Armitage, Stoichiometry and turnover in single, functioning membrane protein complexes, Nature 443 (2006) 355–358.
[49] L.D. Plant, E.J. Dowdell, I.S. Dementieva, J.D. Marks, S.A. Goldstein, SUMO modification of cell surface Kv2.1 potassium channels regulates the activity of rat hippocampal neurons, J. Gen. Physiol. 137 (2011) 441–454.
[50] D. Xiong, T. Li, H. Dai, A.F. Arena, L.D. Plant, S. Goldstein, SUMOylation determines the voltage required to activate cardiac IKs channels, Proc. Natl. Acad. Sci. USA 114 (2017) E6686–E6694.
[51] K. Hines, Inferring subunit stoichiometry from single molecule photobleaching, J. Gen. Physiol. 141 (2013) 737–746.
[52] X.Y. Hua, C.S. Hayes, A. Hofer, B. Fitzsimmons, K. Kilk, U. Langel, T. Bartfai, T. L. Yaksh, Galanin acts at GalR1 receptors in spinal antinociception: synergy with morphine and AP-5, J. Pharmacol. Exp. Ther. 308 (2004) 574–582.
[53] T. Bartfai, U. Langel, K. Bedecs, S. Andell, T. Land, S. Gregersen, B. Ahrén, P. Girotti, S. Consolo, R. Corwin, Galanin-receptor ligand M40 peptide distinguishes between putative galanin-receptor subtypes, Proc. Natl. Acad. Sci. USA 90 (1993) 11287–11291.
[54] J.N. Crawley, J.K. Robinson, U. Langel, T. Bartfai, Galanin receptor antagonists M40 and C7 block galanin-induced feeding, Brain Res 600 (1993) 268–272.
[55] A.M. Mazarati, H. Liu, U. Soomets, R. Sankar, D. Shin, H. Katsumori, U. Langel, C. G. Wasterlain, Galanin modulation of seizures and seizure modulation of hippocampal galanin in animal models of status epilepticus, J. Neurosci. 18 (1998) 10070–10077.
[56] R.L. Parsons, J.M. Mulvaney, L.A. Merriam, Galanin activates an inwardly rectifying potassium conductance and inhibits a voltage-dependent calcium conductance in mudpuppy parasympathetic neurons, Ann. N. Y. Acad. Sci. 863 (1998) 156–169.
[57] L.W. Fitzgerald, J.P. Patterson, D.S. Conklin, R. Horlick, B.L., B.L. Largent, Pharmacological and biochemical characterization of a recombinant human galanin GALR1 receptor: agonist character of chimeric galanin peptides, *J. Pharmacol. Exp. Ther.* 287 (1998) 448–456.
[58] G.A. Kinney, P.J. Emmerson, R.J. Miller, Galanin receptor-mediated inhibition of glutamate release in the arcuate nucleus of the hypothalamus, J. Neurosci. 18 (1998) 3489–3500.
[59] G. Pándy-Szekeres, M. Esguerra, A.S. Hauser, J. Caroli, C. Munk, S. Pilger, G. M. Keserű, A.J. Kooistra, D.E. Gloriam, D. E, The G protein database, GproteinDb, Nucleic Acids Res 50 (2022) D518–D525.